Computer-assisted design of novel polyketide synthase 13 of *Mycobacterium tuberculosis* inhibitors using Molecular modeling and Virtual screening.

.

ABSTRACT

Aims: Polyketide synthase 13 (Pks13) is an essential enzyme in the synthesis of mycolic acids biosynthesis pathway of *Mycobacterium tuberculosis* (Mtb). Therefore, Pks13 is a promising drug target for tuberculosis treatment. Here we report the *in silico* design and evaluation of novel Pks13 inhibitors made of benzofuran derivatives with favorable predicted pharmacokinetic profiles.

Methodology: A 3D model of Pks13-TAMx complexes was prepared for a training set of 18 TAMs with experimentally determined inhibitory potencies (half-maximal inhibitory concentrations IC_{50}^{exp}) by using *in situ* modifications of the crystal structure of the TAM1-Pks13 complex (PDB entry 5V3X). A linear QSAR model was built, correlating computed gas phase enthalpies of formation ($\Delta\Delta H_{MM}$) of Pks13-TAMx complexes with the IC_{50}^{exp} in order to find active conformations of the 18 TAMs. Furthermore, taking into account the implicit solvent effect and entropy changes upon ligand binding, a superior QSAR model was brought forth, correlating computed complexation of Gibbs' free energies $\Delta\Delta G_{com}$. Using the active conformations of the training set TAMs, we built a pharmacophore model (PH4) which was used to virtually screen novel analogs included in a virtual combinatorial library (VCL) of compounds containing benzofuran scaffolds. The PH4 model screened the VCL, which was formerly filtered by Lipinski's rule-of-five, in order to identify new benzofuran analogs.

Results: Gas phase QSAR model: $-\log_{10}(IC_{50}^{exp}) = pIC_{50}^{exp} = -0.1822 \times \Delta\Delta H_{MM} + 6.9135$, $R^2 = 0.89$; superior aqueous phase QSAR model $pIC_{50}^{exp} = -0.2182 \times \Delta\Delta G_{com} + 7.0853$, $R^2 = 0.98$ and PH4 pharmacophore model: $pIC_{50}^{exp} = 1.0003 \times pIC_{50}^{pre} - 0.0019$, $R^2 = 0.91$. The PH4-based screening retained 109 new TAM analogues. Finally, the predicted pharmacokinetic profiles of these new analogues were compared to current orally administered antituberculosis drugs, and the former were found to be almost 92 times more active than TAM2 ($IC_{50}^{exp} = 0.12\mu M$).

Conclusion: This computational approach, which combines molecular mechanics and the Poisson–Boltzmann (PB) implicit solvation theory, the pharmacophore model, the analysis of Pks13-TAMs interaction energies, the in silico screening of VCL compounds, and the inference of ADME properties resulted in a set of new suggested Pks13 inhibitors.

***Keywords**: ADME properties prediction, Polyketide synthase 13, in silico screening, QSAR, Mycobacterium tuberculosis, inhibitors, benzofuran, pharmacophore model.*

1. INTRODUCTION

Tuberculosis is an infectious disease caused by a mycobacterium called Mycobaterium tuberculosis. This mycobacterium belongs to the order of the actinomicetes which is characterized by a thick, very hydrophobic and glycolipid-rich cell wall full of mycolic acids [1].

This disease is airborne through expectorated droplets containing bacilli from people with tuberculosis [2]. It features both an active (contagious) stage and a latent (quasi-asymptomatic, noncontagious) stage during which the bacterium tricks the immune system

with a seemingly sleep phase and the shaping of tuberculous granulomas whereby the bacterium can sporadically be reactivated later [3]. Although pulmonary tuberculosis is the most frequent, there are other forms of disease wherein tuberculous bacilli can spread to other tissues or organs such as the liver and the bones. These kinds of tuberculosis are known as extrapulmonary ones. When several different tissues are simultaneously infected, the disease is then termed disseminated or military [4].

Since 1921, there is a preventive treatment against tuberculosis, precisely the CGB (bacillus Calmette-Guérin) vaccine, which is very effective for children, but not so for teenagers and adults, especially when it comes to the very frequent pulmonary tuberculosis [5]. Current treatments are made of a cocktail of antibiotics administered over a period ranging from six months to two years. Despite the existence of preventive and healing treatments, tuberculosis' occurrence and case-fatality rates remain alarming. In 2020, about 9.9 million people contracted tuberculosis (as opposed to 10 million in 2019) and 1.5 million died thereof (compared to 1.4 million in 2019) [5, 6]. In 2020, according to the WHO report, up to a quarter of the global population is infected with this disease [5]. The fight against tuberculosis faces two major obstacles: AIDS-linked tuberculosis infections and tuberculosis pharmacoresistance. Tuberculosis is the first cause of death among HIV-positive people. As per estimates from 2020, HIV-positive people constituted about a fifth of tuberculosis deaths. When it comes to pharmacoresistance, about half a million people in the whole world in 2019 contracted a rifampicin-resistant tuberculosis strain, 78% of them suffering from a multiresistant tuberculosis [6]. Given such statistics, there is urgent need for newer antituberculous agents with new therapeutical strategies targeting the kind of molecules that are key for the survival of Mycobacterium tuberculosis inside hosts.

M. tuberculosis' cell wall is critical for its viability and virulence. Then, the enzymes responsible for cell wall synthesis are attractive targets for anti-TB drug development [7]. Mycolic acids are long-chain fatty acids which are important for the mycobacterial cell wall's permeability and integrity [8]. Disruption of the mycolic acids' biosynthetic pathway is a strategy for anti-TB drug discovery that has been validated by many of the current first- and second-line anti-TB drugs such as isoniazid, ethionamide, ethambutol, and clinical MmpL3 inhibitor SQ109 [9]. Polyketide synthase 13 (Pks13) performs the final assembly step towards the synthesis of mycolic acids [20]. Pks13 catalyzes a Claisen-type condensation between the carboxyacyl-CoA and meromycoloyl-AMP to produce a mycolic β–ketoester which, in turn, is linked through a thioester bond to the C-terminus (C-ACP) domain of Pks13 [20]. The thioesterase (TE) domain of Pks13 cleaves this thioester bond and forms an ester bond between the mycolic β-ketoester and the Ser 1533 of the TE domain [20]. Then, the Pks13 TE domain forwards the condensation product onto the trehalose in order to synthesize the forerunner of the trehalose monomycolate (TMM). Therefore, Pks13 inhibition interferes with the critical pathway of mycolic acids synthesis, thus killing M. tuberculosis [10, 11]. Only five types of Pks13 inhibitors have been reported so far: thiophene compounds [12, 13], β-lactones [14,15], benzofuran derivatives [16,17], coumestan compounds [18,19], and 4H-chromen-4-one derivatives [20,21]. TAM16 was developed by structure-guided optimization, turning out to be a promising candidate with potent efficacy in both acute and chronic mouse TB infection models along with favorable druggability [17].

In this work, our goal is to conceive new analogs of benzofuran derivatives out of a series of 18 training set and 5 validation set known inhibitors with known experimental inhibitory activities [17]. Information about the structure and the experimental activities (IC_{50}^{exp}) of this series of Pks13-inhibiting molecules have been provided by Aggarwal et al. [17]. In order to reach our goal, we will first elaborate a QSAR model correlating the amount of Gibbs' free energy made available by the shaping of the Pks13-TAMs complexes with their respective experimental activities, and then a 3D QSAR pharmacophore (PH4) model of Pks13 inhibition based on the active conformations obtained by the complexation method. Right afterwards, we generate and screen a virtual library using the generated PH4. And we finally

evaluate the predicted activity of the best PH4-based analogs and compute their ADME profile subsequently.

2. MATERIAL AND METHODS

2.1 Training and Validation Sets

The dataset including chemical structures and biological activities (IC_{50}^{exp}) of benzofuran derivatives inhibitors of Pks13 used in this work, were taken from the article published by Aggarwal et *al.* [11].
These compounds span a large range of half-maximal inhibitory concentrations ($0.12 \leq IC_{50}^{exp} \leq 35.8\mu M$) to allow the design of a QSAR model. This dataset was split into a training set (TS) containing 18 benzofuran inhibitors and a validation set (VS) including 5 benzofuran inhibitors by a protocol called « Generate training and test data », within the Discovery Studio 2016 software.

2.2 Model Building

3D molecular models of enzyme-inhibitor (E-I) complexes Pks13-TAMx, free Pks13 enzymes and free TAM inhibitors were prepared from the high-resolution (1.94 Å) crystal structure of a reference complex containing the training set compound TAM1 bound to the Pks13 (Protein Data Bank entry code 5V3X [17]) using the Insight-II molecular modeling program [22].
The structures of Pks13 and of the E-I complexes whose pH stood at 7, and whose N- and C-terminal residues were neutral, had all their protonizable and ionizable residues charged. All water molecules were removed from the crystal structure. The inhibitors were built into the reference structure 5V3X [17] by continuously in situ changing derivatized groups in the molecular scaffold of the template inhibitor TAM1. An exhaustive conformational search over all rotatable bonds of the replacing function groups, along with a meticulous gradual energy-minimization of the modified inhibitor and of active site residues of the Pks13 within 5Å of the inhibitor, helped us find low-energy bound conformations of the modified inhibitor. The subsequent low-energy structures of the E-I complexes were then refined by minimizing the whole complex. This procedure has been often used with much success to build models of viral, bacterial and protozoal enzyme-inhibitor complexes and to design peptidomimetic, hydroxynaphthoic, thymidine, triclosan, pyrrolidine carboxamide, nitriles and chalcone-based inhibitors [23-33].

2.3 Molecular Mechanics

The modeling of inhibitors, Pks13 and E-I complexes was carried out by molecular mechanics as described earlier [23].

2.4 Conformational Search

As mentioned earlier, free inhibitor conformations were derived from their bound conformations in the E-I complexes through gradual relaxation to the nearest local energy minimum [23].

2.5 Solvation Gibbs' Free Energies

The electrostatic component of solvation Gibbs free energy (GFE), which also includes the effects of ionic strength through the solution of the nonlinear Poisson–Boltzmann equation [34,35] was computed by the Delphi module in Discovery Studio [36] as aforementioned [23].

2.6 Calculation of Binding Affinity and QSAR Model

The computation of binding affinity expressed by the GFE complexation has been discussed in more depth earlier [23].

2.7 Interaction Energy

The computation of MM interaction energy (E_{int}) between enzyme residues and the inhibitor CFF97 force field was performed as described earlier [23].

2.8 Pharmacophore Generation

Bound conformations of inhibitors out of the models of E-I complexes were used to build a 3D-QSAR pharmacophore (PH4) model via the Catalyst HypoGen algorithm [27] implemented in Discovery Studio [38] as described earlier [23].

2.9 ADME Properties

The pharmacokinetic profile of TAMs were computed by the QikProp program [38] as described earlier [23].

2.10 Virtual Library Generation

The virtual library generation was performed as described earlier [23].

2.11 ADME-Based Library Searching

The drug-likeness selection criterion served to downsize the initial virtual library into one that's more useful for our purposes [23].

2.12 Pharmacophore-Based Library Searching

The pharmacophore model (PH4) described in Section 2.8 and derived from the bound conformations of TAMs at the active site of Pks13 made up the library searching tool, as described earlier [23].

2.13 Inhibitory Potency Prediction

The conformer with the best mapping on the PH4 pharmacophore in each cluster of the focused library subset was used to compute $\Delta\Delta G_{com}$ and IC_{50}^{exp} estimation (virtual screening) through the complexation QSAR model as described earlier [23].

.

3. RESULTS AND DISCUSSION

3.1 Training and Validation Sets

The training set of 18 TAMs and the validation set of 5 TAMs (Table 1) were selected from the work of Aggarwal et *al.* [17]. Substitutions made at five positions R1, R2, R3, 5'and 6' of the benzofuran scaffold and R -group, as shown in (Table 1), made up the entire series. The experimental half-maximal inhibitory concentrations ($0.12 \leq IC_{50}^{exp} \leq 35.80\,\mu M$) [17] cover a sufficiently wide concentration range to build a reliable QSAR model.

Table 1. Training Set (TS) and validation set (VS) of benzofuran derivatives inhibitors of Pks13 [17] used in the preparation of QSAR models of inhibitor binding. The R-groups are numbered as #R ≡ group index.

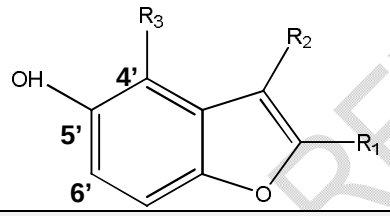

#R	1	2	3	4	5
R group	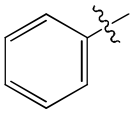	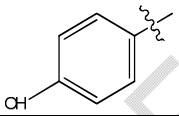	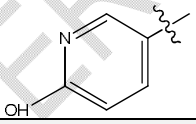	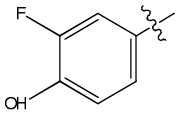	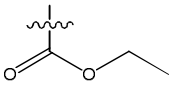
#R	**6**	**7**	**8**	**9**	**10**
R group	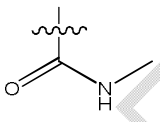	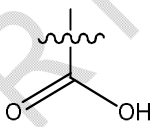	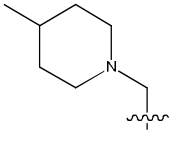	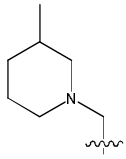	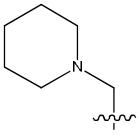
#R	**11**	**12**	**13**	**14**	**15**
R group	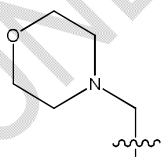	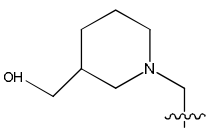	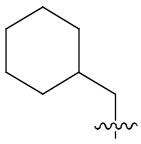	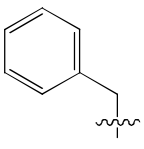	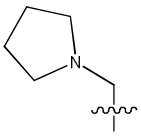
#R	**16**	**17**	**18**		
R group	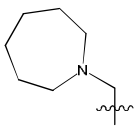	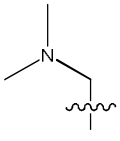	H		

Training Set	TAM1	TAM2	TAM3	TAM4	TAM5	TAM6
#R_1-#R_2-#R_3	1-5-8	1-5-9	1-5-15	1-5-16	1-5-11	1-5-17
IC_{50}^{exp} (μM)	0.26	0.12	0.24	0.28	0.71	1.57
Training set	**TAM8**	**TAM9**	**TAM11**	**TAM12**	**TAM13**	**TAM14** [a]
#R_1-#R_2-#R_3	1-5-14	1-5-10	1-5-13	1-6-10	2-5-10	1-5-10
IC_{50}^{exp} (μM)	11.90	0.26	19.60	0.29	0.17	35.80
Training set	**TAM15** [b]	**TAM17**	**TAM18**	**TAM20** [c]	**TAM21**	**TAM23**
#R_1-#R_2-#R_3	1-5-10	3-5-10	4-6-10	2-5-10	1-5-12	2-5-12
IC_{50}^{exp} (μM)	2.00	0.36	0.33	0.45	0.42	0.28
Validation Set	TAM7	TAM10	TAM16	TAM19 [c]	TAM24	
#R_1-#R_2-#R_3	1-5-18	1-7-10	2-6-10	2-6-10	1-6-12	
IC_{50}^{exp} (μM)	20.00	6.60	0.19	0.57	2.10	

[a] *TAM14:* ***5'*** *– MeO;* [b] *TAM15:* ***5'*** *– H;* [c] *TAM19 and TAM20:* ***5'*** *– H,* ***6'*** *– OH.*

3.2 QSAR Model

3.2.1 Single-descriptor QSAR models

Each of the 18 training sets (TS) and 5 validation sets (VS) of Pks13-TAMs complexes (table 1) was prepared by *in situ* modification of the refined template crystal structure (pdb entry code 5v3x [17]) of the complex Pks13-TAM1 as described in the Methods section. Further, the relative Gibbs free energy of the Pks13-TAMx upon complex formation ($\Delta\Delta G_{com}$) was computed for each of the 23 optimized enzyme–inhibitor complexes. (Table 2) lists computed values of $\Delta\Delta G_{com}$ and its components for the TS and VS of benzofuran derivatives [11]. The QSAR model explained variation in the TAMs experimental inhibitory potencies ($pIC_{50}^{exp} = -\log_{10}(IC_{50}^{exp})$ [17]) by correlating it with computed GFE $\Delta\Delta G_{com}$ through a linear regression. In addition, significant correlation obtained in this QSAR relationship permitted to determine the active bound conformation of the TAMs at the Pks13 binding site and enabled generation of PH4 pharmacophore inhibition. In search for better insight into the binding affinity of TAMs towards Pks13, we have analyzed the enthalpy of complexation in gas phase $\Delta\Delta H_{MM}$ by correlating it with the pIC_{50}^{exp}. The validity of this linear correlation allowed assessment of the significance of inhibitor-enzyme interactions ($\Delta\Delta H_{MM}$) when solvent effect and loss of entropy of the inhibitor upon binding to the enzyme were neglected. For statistical data of the regression, see Table 3, Equation A. This correlation explained about 89% of the variation in pIC_{50}^{exp} data and underlined the role of the enthalpic contribution to the binding affinity of the ligand. More, the advanced descriptor, namely the GFE of the Pks13-TAMx complex formation including all components: $\Delta\Delta H_{MM}$, $\Delta\Delta TS_{vib}$ and $\Delta\Delta G_{sol}$, has been assessed (for statistical data see Table 3, Equation B). Relatively high values of the regression coefficient R^2, adjusted R_{xv}^2 and Fischer F-test of the correlation

show the importance of the entropic term in a biological environment and suggest a good relationship between the 3D model of inhibitor binding and the observed inhibitory potencies of the TAMx [17] .Therefore, structural information derived from the 3D models of Pks13–TAMx complexes is expected to lead to reliable predictions of Pks13 inhibitory potencies for novel benzofuran analogs based on the QSAR model B (Table 3).

Table 2. Gibbs free energy (binding affinity) and its components for the training set of Pks13 inhibitors and validation set inhibitors [17]

Training Set [a]	M_W [b] [g.mol^{-1}]	$\Delta\Delta H_{MM}$ [c] [kcal.mol^{-1}]	$\Delta\Delta G_{sol}$ [d] [kcal.mol^{-1}]	$\Delta\Delta TS_{vib}$ [e] [kcal.mol^{-1}]	$\Delta\Delta G_{com}$ [f] [kcal.mol^{-1}]	IC_{50}^{exp} [g] [µM]
TAM1	393.48	3.84	-2.98	-1.10	1.96	0.26
TAM2	393.48	0.00	0.00	0.00	0.00	0.12
TAM3	365.42	0.82	-0.23	-1.43	2.02	0.24
TAM4	393.48	1.95	-0.87	-1.41	2.49	0.28
TAM5	381.42	5.16	-2.52	-1.79	4.43	0.71
TAM6	339.39	5.73	-0.80	-0.92	5.85	1.57
TAM8	372.41	7.21	-3.06	-5.11	9.26	11.90
TAM9	379.45	0.81	-0.28	-1.65	2.18	0.26
TAM11	378.46	13.09	-3.71	-1.76	11.14	19.60
TAM12	364.44	1.72	0.44	-0.74	2.90	0.29
TAM13	395.45	-0.11	0.21	-1.46	1.56	0.17
TAM14	393.48	12.79	-3.35	-2.11	11.55	35.80
TAM15	363.45	6.49	0.97	0.26	7.20	2.00
TAM17	396.44	4.09	-2.74	-1.88	3.23	0.36
TAM18	398.43	3.84	-2.09	-1.38	3.13	0.33
TAM20	395.45	3.79	-2.00	-1.35	3.14	0.45
TAM21	409.48	2.68	-0.96	-1.29	3.01	0.42
TAM23	425.47	3.29	-0.52	-0.80	3.57	0.38
Validation Set[a]	M_W [b] [g.mol^{-1}]	$\Delta\Delta H_{MM}$ [c] [kcal.mol^{-1}]	$\Delta\Delta G_{sol}$ [d] [kcal.mol^{-1}]	$\Delta\Delta TS_{vib}$ [e] [kcal.mol^{-1}]	$\Delta\Delta G_{com}$ [f] [kcal.mol^{-1}]	pIC_{50}^{pre}/ pIC_{50}^{exph}
TAM7	282.29	9.93	-1.71	-4.30	12.52	0.93
TAM10	351.40	9.04	-2.66	-1.82	8.20	1.02
TAM16	380.44	0.18	0.71	-0.48	1.37	1.01
TAM19	380.44	4.57	-0.98	-0.66	4.25	0.99
TAM24	394.46	5.84	-0.89	-1.94	6.89	0.98

[a] *for the chemical structures of training set and validation set see (Table 1) ;* [b] *Mw is the molar mass of inhibitors ;* [c] *$\Delta\Delta H_{MM}$ is the relative enthalpic contribution to the GFE change related to E:I complex formation derived by MM ;* $\Delta\Delta H_{MM} \cong [E_{MM}\{E{:}I_x\} - E_{MM}\{I\}_x] - [E_{MM}\{E{:}I_{ref}\} - E_{MM}\{I_{ref}\}]$, I_{ref} *is the reference inhibitor TAM2 ;* [d] *$\Delta\Delta G_{sol}$ is the relative solvation Gibbs free energy contribution to the Gibbs free energy related to E:I complex formation :* $\Delta\Delta G_{sol} = [G_{sol}\{E{:}I_x\} - G_{sol}\{I\}_x] - [G_{sol}\{E{:}I_{ref}\} - G_{sol}\{I_{ref}\}]$; [e] *$\Delta\Delta TS_{vib}$ is the relative entropic contribution of the inhibitor to Gibbs free energy to E:I complex formation :* $\Delta\Delta TS_{vib} = [\Delta\Delta TS_{vib}\{I_x\}_E - \Delta\Delta TS_{vib}\{I_x\}] - [\Delta\Delta TS_{vib}\{I_{ref}\}_E - \Delta\Delta TS_{vib}\{I_{ref}\}]$; [f] *$\Delta\Delta G_{com}$ is the relative Gibbs free energy related to E:I complex formation :* $\Delta\Delta G_{com} \cong \Delta\Delta H_{MM} + \Delta\Delta G_{sol} - T\Delta\Delta S_{vib}$; [g] IC_{50}^{exp} *is the experimental half-maximal inhibition concentration obtained from reference [11] ;* [h] *ratio of predicted and experimental half-maximal concentrations* $pIC_{50}^{pre}/pIC_{50}^{exp}$. $pIC_{50}^{Exp} = -log_{10}(IC_{50}^{exp})$ *was predicted from computed $\Delta\Delta G_{com}$ using the regression equation for Pks13 show in (table 3, B).*

Table 3. Analysis of computed binding affinities $\Delta\Delta G_{com}$, its enthalpic component $\Delta\Delta H_{MM}$ and experimental half-maximal inhibitory concentrations $pIC_{50}^{exp} = -\log_{10}(IC_{50}^{exp})$ of TAMs towards Pks13 [17]

Statistical Data of Linear Regression	A	B
$pIC_{50}^{exp} = -0.1822 \times \Delta\Delta H_{MM} + 6.9135$ (A)		
$pIC_{50}^{exp} = -0.2182 \times \Delta\Delta G_{com} + 7.0853$ (B)		
Number of compounds n	18	18
Squared correlation coefficient of regression R^2	0.89	0.98
LOO cross-validated squared correlation coefficient R^2_{xv}	0.87	0.98
Standard error regression σ	0.24	0.09
Statistical significance of regression, Fisher F-test	136.85	1008.07
Leve of statistical significance α	> 95%	
Range of activities IC_{50}^{exp} [µM]	0.12 - 35.80	

The statistical data confirmed the validity of the correlation. Equations (A) and (B) are plotted on (Figure 1). The ratio $pIC_{50}^{pre}/pIC_{50}^{exp} \cong 1$ (the pIC_{50}^{pre} values were estimated using correlation Equation B, Table 3) calculated for the validation set TAM7, TAM10, TAM16, TAM19, TAM24 documents the substantial predictive power of the complexation QSAR model from Table 2. Thus, the regression Equation B (Table 3) and computed GFE $\Delta\Delta G_{com}$ can be used for prediction of inhibitory potencies IC_{50}^{exp} against Pks13 for novel benzofuran analogs provided they share the same binding mode as the training set.

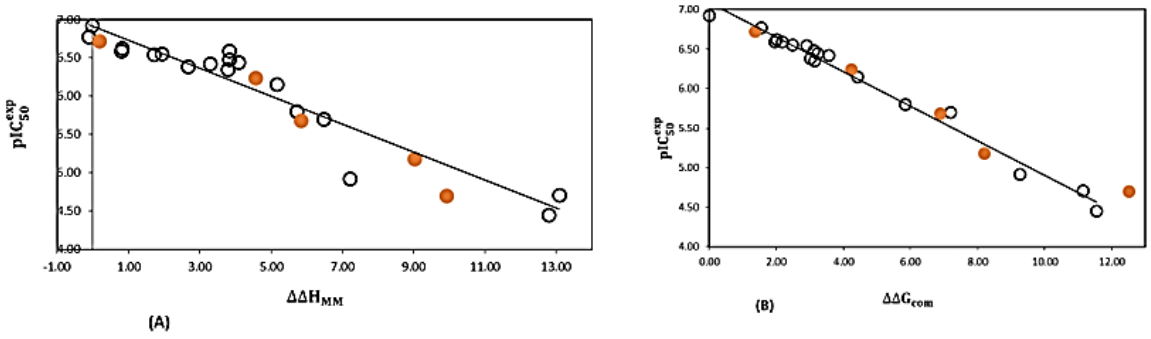

Fig. 1. (A) Plot of correlation equation between pIC_{50}^{exp} and relative enthalpic contribution to the GFE $\Delta\Delta H_{MM}$ [kcal.mol^{-1}] (B) Similar plot for relative complexation Gibbs free energies of the Pks13-TAMx complex formation $\Delta\Delta G_{com}$ [kcal.mol^{-1}] of the training set [17].

The validation set data points are shown in red color.

3.2.2 Binding mode of TAMs

The structural information from the Pks13-TAMx complexes help identify key interactions which explain the affinity of benzofuran derivatives with Pks13. In fact, the key interactions

which are involved in the shaping of Pks13-TAMx complexes and which justify the affinity of benzofuran derivatives with Pks13, are hydrogen bonds, Van der Waals and hydrophobic contacts, etc. As shown on Figure 2, several residues interact with TAM2: hydrogen bonds with residues Asp1644 and Asn1640 along with Van der Waals interaction with Tyr1663, π-π stacking with Tyr1582 and Phe1670 and hydrophobic contacts with residues Ile1643 and Ala1667. Most training set molecules share these interactions enumerated for TAM2. On the other hand, some of these interactions are loss for less active training set compounds (TAM14, TAM15, TAM6) or the van der Waals and stacking interactions with other residues such as Tyr1663 and Tyr1674. For other less active molecules (TAM11, TAM8) the cyclical fragments at location R_3 of the benzofuran scaffold lack the nitrogen atom needed to retain one of the key hydrogen bond with the Asn1640 residue. Indeed, the Asp1644, Tyr1674, Tyr1663 and Asn1640 residues are among the key residues for the affinity of benzofuran derivatives for Pks13 [17,21]. In this work, interactions with these residues have been successfully preserved.

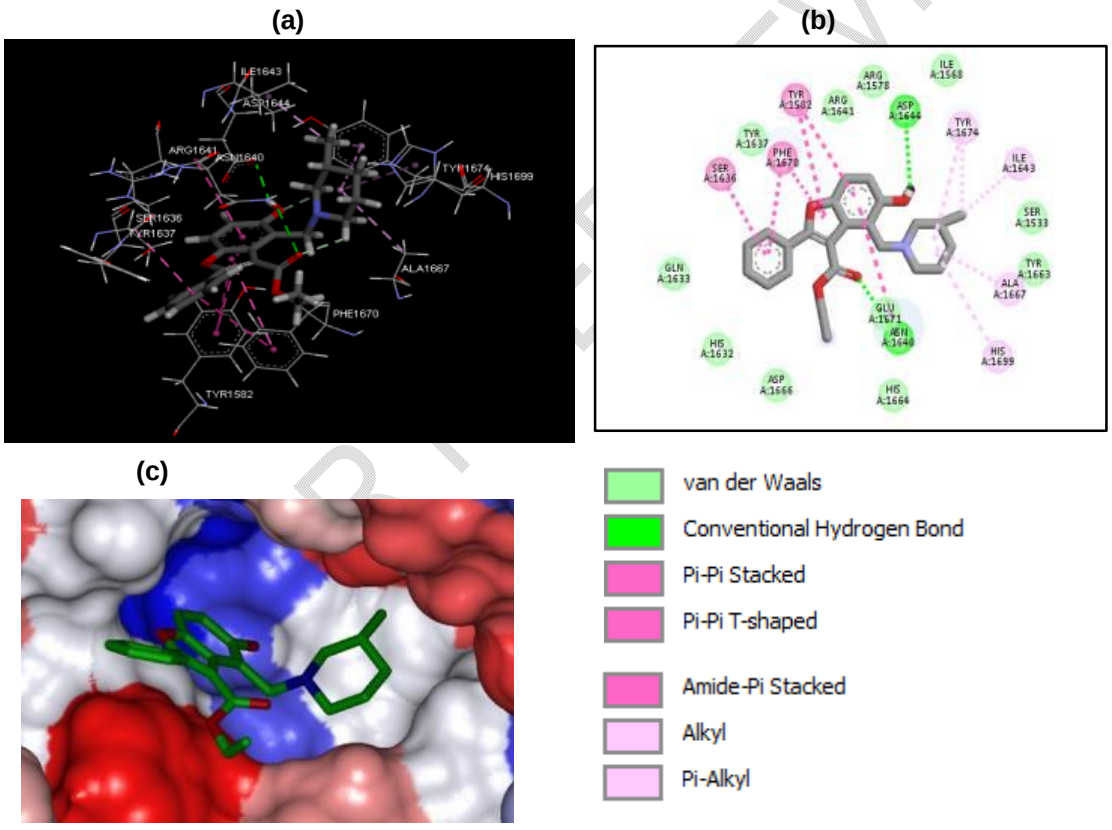

Fig. 2. (a) 3D structure of the Pks13 active site with bond inhibitor TAM2; (b) 2D schematic interaction diagram of the most potent inhibitor TAM2 [11] at the active site; (c) Connolly surface of the pks13 active site for TAM2. surface coloring legend: red=hydrophobic, blue= hydrophilic and white= intermediate.

3.2.3 Interaction Energy

Additional information about the interaction mode of the ligands of the training set are provided by the interaction energies diagram. This diagram is derived from the individual energetic contributions of each Pks13 active site residue with the training set ligands. The breakout of the interaction energy into individual contributions of the residuals of the Pks13 active site is important in picking substitutes for the improvement of the binding affinity of benzofuran analogs with Pks13 to strengthen their inhibitory ability. The individual contributions of the interaction energies are classified into the three following groups according to the activity level of the training set ligands: the most active ligands, the moderately active ligands and the least active ligands (figures 3: (a), (b) and (c)). The comparative analysis of these contributions with respect to their interaction energies facilitates the identification of the residues the contribution of which to binding affinity is most significant. Upon analyzing it further, we notice that the level of contribution with respect to the interaction energies of Pks13 active site residues is almost the same for the three categories of inhibitors. And so, we make no specific suggestion for substitutions able to potentially improve binding affinity. In designing new inhibitors out of benzofuran derivatives, a (so-named) combinatory approach is adopted. Through this approach, we generated an *in silic*o library screening of 169,136 benzofuran analogs.

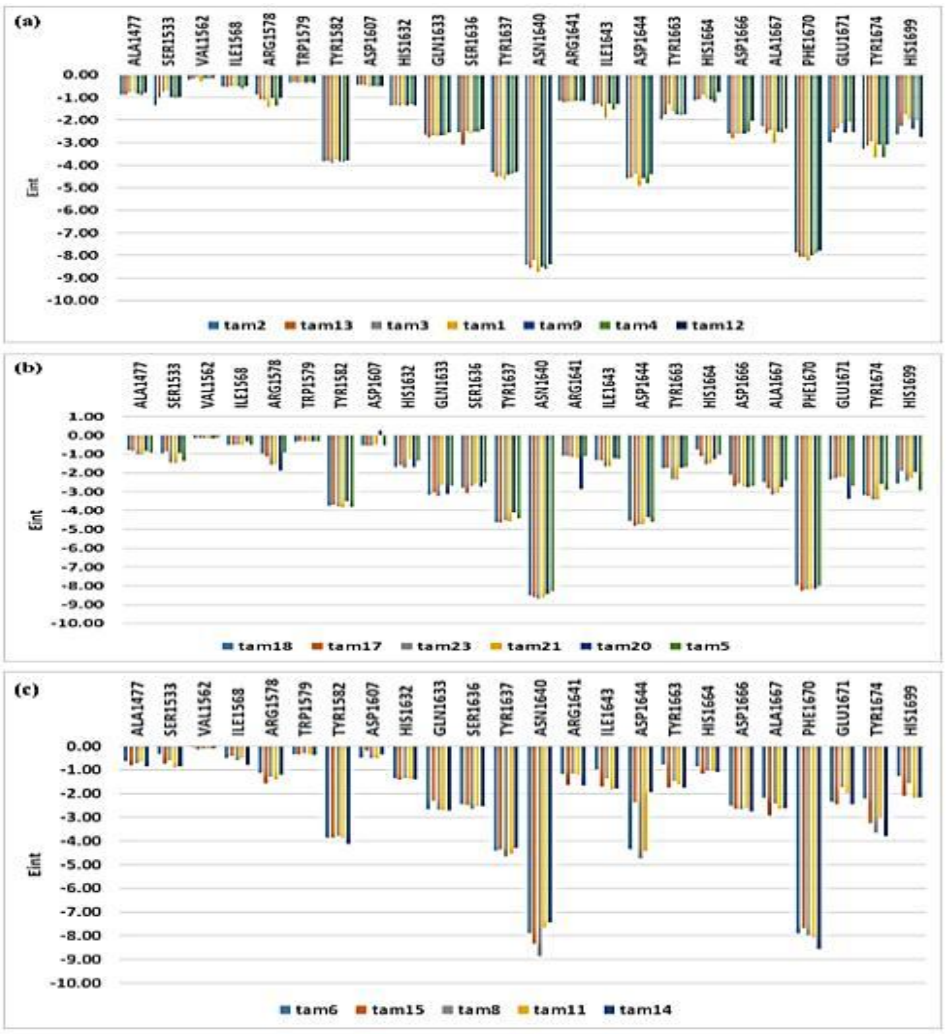

Fig. 3. Molecular mechanics intermolecular interaction energy breakdown to residue contributions in [kcal.mol^{-1}] :(a) the most active inhibitors; (b) moderately active inhibitors; (c) less active inhibitors, (Table 2) [17].

3.3 3D-QSAR Pharmacophore Model

The 3D-QSAR pharmacophore model of Pks13 is elaborated from the active conformations of the training set ligands and the ligands of the validation set. The generation process of the pharmacophore model based on the Catalyst HypoGen algorithm (in Discovery Studio 2.5), is conducted through three consecutive steps: the constructive step, the subtractive step and the optimization step [39]. During the constructive step, one of the training set molecules TAM2 has been selected to generate pharmacophore hypotheses for it alone yielded an activity which fits the threshold criterion: $IC_{50}^{exp} \leq 1.26 \times 0.12\ \mu M$;
In the subtractive stage, the features available in more than half of the inactive molecules are withdrawn. Then the hypotheses generated from these molecules which lost no features

are kept aside. A molecule is deemed inactive by the HypoGen algorithm when its inhibitory activity fulfills the following condition: $IC_{50}^{exp} > 0.12 \times 10^{3.5}\mu M = 379.47\mu M$

Given that principle, no molecule from the training set was classified as inactive. As a result, no initial PH4 feature was lost. At the optimization stage, the remaining hypotheses are optimized and the 10 best are selected. The cost values, the correlation coefficients; the root-mean-square deviations (RMSD), the pharmacophores' features and the maximal adjustment value of the 10 highest-ranked hypotheses are compiled in the (table 4).

These 10 hypotheses have been selected according to their statistical parameters such as a high R^2 correlation coefficient, a low total cost value and a low root-mean-square. After its conception, the pharmacophore model has been afterwards evaluated for its reliability on the basis of the parameters of computed costs ranging from 82.64 (Hypo1) to 169.80 (Hypo10). The relatively low gap between the parameter of the highest cost and that of the least predictably fits the homogeneity of the generated hypotheses and the coherence of the training set molecules. For this PH4 pharmacophore model, the difference between the cost of each hypothesis and the null cost is superior to 82. Also, the fixed cost (42.14) is inferior to the null cost (481.72) with a difference of Δ = 439.58. The fact that this difference is superior to 70 ($\Delta > 70$), means that the odds are strong; precisely better than 90%, that the pharmacophore model is predictive and represents a true correlation [39]. In order to be statistically significant, a hypothesis must have a total cost closer to the fixed cost and further from the null one. For these 10 hypotheses altogether, the difference between the null cost and the total cost is superior or equal to 311.92, which illustrates the high quality of this pharmacophore model. The RMSD between the hypotheses ranges from 2.12 to 3.75 and the R^2 correlation coefficient is situated between 0.85 and 0.95. The first hypothesis (Hypo1) totaling a cost of 82.64 which is the closest to the fixed cost (42.14) and the furthest from the null cost (481.72), the best RMSD (2.12) and the best R^2 (0.95) has been selected for a deeper analysis. The configuration cost (8.53 for all hypotheses) being inferior to 17 confirms this pharmacophore as reasonable [39].

What links the confidence level 98% and the number of 49 random executions for each hypothesis is based on the following formula**:** $S = \left[1 - \frac{1+X}{Y}\right] \times 100$ [39].

Whereby X is the total number of hypotheses whose total cost is inferior to that of the initial hypothesis (Hypo1) and Y the total number of HypoGen executions (initial execution + random executions): X = 0 et Y = (1 + 49), so $98\% = \left[1 - \frac{1+0}{1+49}\right] \times 100$ **.**

The first hypothesis has been evaluated by a Fischer-test. The Cat Scramble program has been used to randomly sample the experimental activities of all the training set molecules. At a 98% confidence level, each of the 49 random executions resulted in 10 valid hypotheses, using the same characteristics and parameters as these of the generation of the 10 hypotheses of the initial pharmacophore. Among them, the value of the cost of the first hypothesis is the lowest, as opposed to the 49 randomly generated hypotheses ; as we can observe in (Table 4) where the lowest cost of the 49 random executions is compiled for each initial hypothesis, and none of them was as predictive as the initial generated hypotheses displayed in table 4.

Thus, there is a 98% chance that the first hypothesis constitutes a pharmacophore model of the inhibitory activity of the benzofuran derivatives with a comparable predictive power to that of the QSAR model of complexation in an aqueous environment. Another evaluation of the first hypothesis is the mapping of the most active ligand (TAM2) of the training set (Figure 4).

Table 4. Parameters of 10 generated PH4 pharmacophoric hypotheses for Pks13 inhibitors [17] after the Cat Scramble validation procedure (49 scrambled runs for each hypothesis at the selected level of confidence of 98%)

Hypothesis	RMSD [a]	R^2 [b]	Total Cost [c]	Costs Difference [d]	Closest Random [e]
Hypo1	2.12	0.95	82.64	399.08	186.17
Hypo2	2.26	0.95	87.92	393.79	254.60
Hypo3	2.55	0.93	100.63	381.09	299.02
Hypo4	3.30	0.88	140.83	340.89	317.62
Hypo5	3.36	0.88	144.68	337.03	322.95
Hypo6	3.56	0.86	157.16	324.55	323.07
Hypo7	3.65	0.86	163.91	317.80	323.46
Hypo8	3.72	0.85	167.91	313.81	334.99
Hypo9	3.72	0.85	167.91	313.81	335.53
Hypo10	3.75	0.85	169.80	311.92	336.90

[a] Root Mean Square Deviation; [b] Squared correlation coefficient; [c] Overall cost parameter of the pharmacophore (PH4); [d] Cost difference between Null cost and hypothesis total cost; [e] Lowest cost from 49 scrambled runs at a selected level of confidence of 98%. The Fixed Cost = 42.14 with RMSD = 0, the Null Cost = 481.72 with RMSD = 7,07 and the Configuration cost = 8.53.

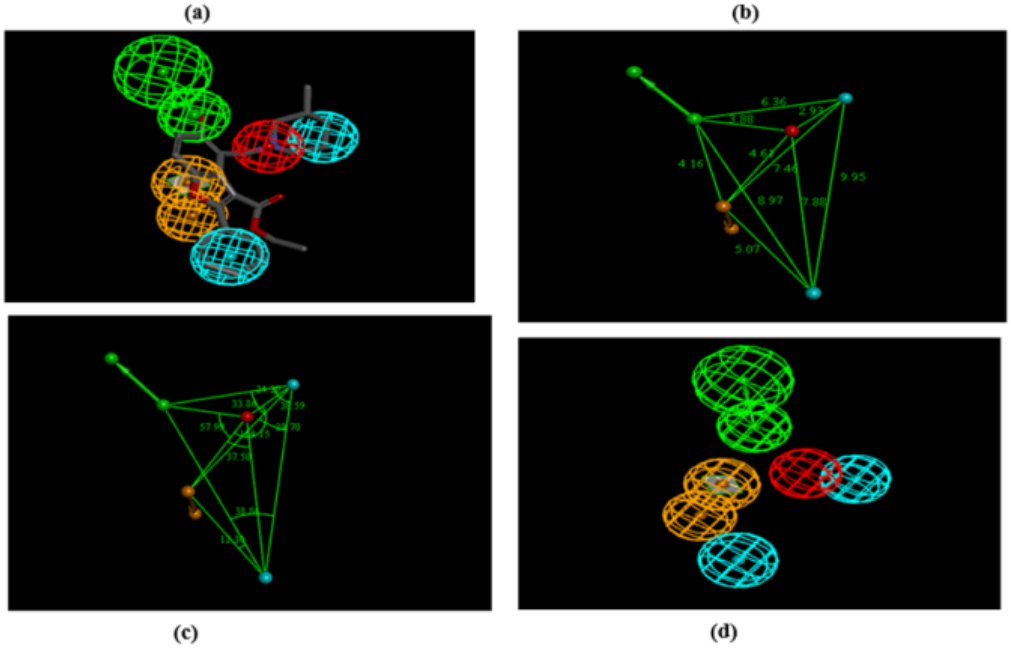

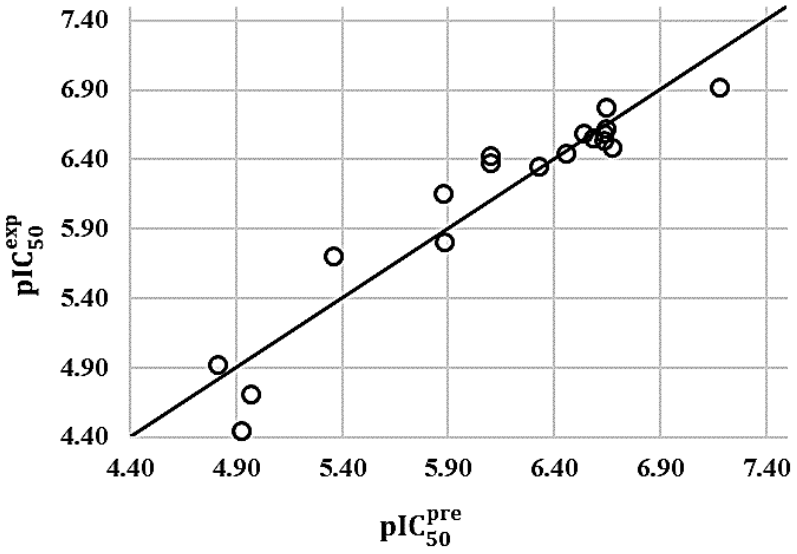

(e)

Fig. 4. shows (a) features of the pharmacophore model of Pks13 inhibition; (b) distances between centers; (c) angle between centers of pharmacophoric features; (d) pharmacophore mapping with the most potent molecule TAM2 ($IC_{50}^{exp} = 0.12\mu M$). The features are colored green for Hydrogen Bond Acceptor (HBA), orange for aromatic ring (Ar), blue for hydrophobic and red for pos ionizable; (e) correlation plot of experimental Vs. predicted inhibitory activity (open circles correspond to TS).

Then, a linear regression was computed between the experimental biological activities and the ones predicted by the first hypothesis in order to measure the predictable power of the pharmacophore. The following equation for the line of best fit has been obtained as follows: $pIC_{50}^{exp} = 1.0003 \times pIC_{50}^{pre} - 0.0019$ (n = 18, R^2= 0.91, R_{xv}^2= 0.87, σ = 0.22, F-test = 161.48, α > 98%) is also plotted in (Figure 4).

3.4 Virtual Screening

The *in silico* screening of a (combinatory) virtual library can facilitate the identification of better outcomes, as was shown in the works of Kouassi et *al.* [40], N'Guessan et *al.* [23] and Allangba et *al.* [36] about the design.

3.4.1 Virtual library

The substitutions at positions R_1, R_2 and R_3 of the skeleton of the endogenous ligand (TAM2) of the training set allowed us to generate a virtual library of the size R_1 x R_2 x R_3 = 248 x 22 x 31 = 169,136 benzofuran analogs.

The names of the R_1, R_2 and R_3 fragments are mentioned in the (Table 5). In order to conceive new drug-like analogs which are also orally administrable, the Lipinski's rule of five [41] has been applied to the library's 169,136 analogs. This first focusing led to a relatively smaller library containing only 10,919 analogs. This downsized library then went through *in silico* screening.

Table 5. R1 to R3 -groups (fragments, building blocks, substituents) used in the design of the initial diversity virtual combinatorial library of benzofuran derivatives

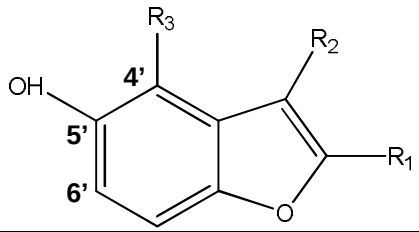

R-groups *					
1	3-ethylphenyl	2	3-ethyl-4-hydroxyphenyl	3	4-hydroxy-3-isopropylphenyl
4	3-isopropylphenyl	5	3-ethyl-5-methylphenyl	6	3-ethyl-4-hydroxy-5-methylphenyl
7	3-isopropyl-5-methylphenyl	8	3-ethyl-4-isopropylphenyl	9	5-ethyl-2-hydroxy-4-isopropylphenyl
10	5-ethyl-2,4-dihydroxyphenyl	11	3-ethyl-cyclohexyl	12	3-ethyl-5-methylcyclohexyl
13	5-ethyl-2,4-dihydroxycyclohexyl	14	3-isopropylcyclohexyl	15	3-isopropyl-5-methylcyclohexyl
16	3-ethyl-4-isopropylcyclohexyl	17	5-ethyl-2-hydroxy-4-isopropylcyclohexyl	18	5-ethyl-2-hydroxycyclohexyl
19	2-hydroxy-5-isopropylcyclohexyl	20	3-ethylpiperidin-1-yl	21	3-ethyl-5-methylpiperidin-1-yl
22	3-isopropylpiperidin-1-yl	23	2-hydroxy-5-isopropylpiperidin-1-yl	24	5-ethyl-2-hydroxypiperidin-1-yl
25	3-ethyl-4-hydroxypiperidin-1-yl	26	3-ethyl-4-isopropylpiperidin-1-yl	27	5-ethyl-2-hydroxyl-3-mehtylpiperidin-1-yl
28	5-ethyl-2-hydroxy-4-isopropylpiperidin-1-yl	29	3-ethyl-4-methoxypiperidin-1-yl	30	5-ethyl-2-hydroxyphenyl
31	2-hydroxy-5-isopropylphenyl	32	4-(1H-pyrrol-3-yl)phenyl	33	4-(furan-3-yl)phenyl
34	4-(1H-pyrrol-1-yl)phenyl	35	3-ethyl-4-(1H-pyrrol-1-yl)phenyl	36	2-hydroxy-4- (1H-pyrrol-1-yl)phenyl
37	5-ethyl-2-hydroxy-4-(1H-pyrrol-1-yl)phenyl	38	2-hydroxy-5-isopropyl-4-(1H-pyrrol-1-yl)phenyl	39	3-isopropyl-4-(1H-pyrrol-1-yl)phenyl
40	3-ethyl-4-(1H-pyrrol-3-yl)phenyl	41	5-ethyl-2-hydroxy-4-(1H-pyrrol-3-yl)phenyl	42	2-hydroxy-5-isopropyl-4-(1H-pyrrol-3-yl)phenyl

43	3-isopropyl-4-(1H-pyrrol-3-yl)phenyl	44	4-(3-hydroxy-1H-pyrrol-1-yl)phenyl	45	3-ethyl-4-(3-hydroxy-1H-pyrrol-1-yl)phenyl
46	5-ethyl-2-hydroxy-4-(3-hydroxy-1H-pyrrol-1-yl)phenyl	47	2-hydroxy-4-(3-hydroxy-1H-pyrrol-1-yl)-5-isopropylphenyl	48	4-(3-hydroxy-1H-pyrrol-1-yl)-3-isopropylphenyl
49	3-ethyl-4-(furan-3-yl)phenyl	50	5-ethyl-4-(furan-3-yl)-2-hydroxyphenyl	51	4-(furan-3-yl)-2-hydroxy-5-isopropylphenyl
52	4-(furan-3-yl)-3-isopropylphenyl	53	5-ethyl-2-methylphenyl	54	5-ethyl-2,3-dimethylphenyl
55	5-ethyl-2-hydroxy-3-methylphenyl	56	3-ethylcycloheptyl	57	6-ethyl-2-methylcycloheptyl
58	3-ethyl-6-methylcycloheptyl	59	3-ethyl-5-methylcycloheptyl	60	6-ethyl-2-hydroxycycloheptyl
61	6-ethyl-2-hydroxy-3-methylcycloheptyl	62	6-ethyl-2-hydroxy-4-methylcycloheptyl	63	6-ethyl-2-hydroxy-3,4-dimethylcycloheptyl
64	3-isopropylcycloheptyl	65	6-isopropyl-2-methylcycloheptyl	66	3-isopropyl-6-methylcycloheptyl
67	3-isopropyl-5-methylcycloheptyl	68	6-isopropyl-2,4-dimethylcycloheptyl	69	6-isopropyl-3,4-dimethylcycloheptyl
70	6-isopropyl-2,3-dimethylcycloheptyl	71	2-hydroxy-6-isopropylcycloheptyl	72	2-hydroxy-6-isopropyl-3-methylcycloheptyl
73	2-hydroxy-6-isopropyl-3,4-dimethylcycloheptyl	74	2-hydroxy-6-isopropyl-4-methylcycloheptyl	75	3-ethylazepan-1-yl
76	6-ethyl-2-methylazepan-1-yl	77	3-ethyl-6-methylazepan-1-yl	78	3-ethyl-5-methylazepan-1-yl
79	6-ethyl-2,4-dimethylazepan-1-yl	80	6-ethyl-2,3-dimethylazepan-1-yl	81	6-ethyl-3,4-dimethylazepan-1-yl
82	6-ethyl-2-hydroxyazepan-1-yl	83	6-ethyl-2-hydroxy-3-methylazepan-1-yl	84	6-ethyl-2-hydroxy-4-methylazepan-1-yl
85	6-ethyl-2-hydroxy-3,4-dimethylazepan-1-yl	86	3-isopropylazepan-1-yl	87	6-isopropyl-2-methylazepan-1-yl
88	3-isopropyl-6-methylazepan-1-yl	89	3-isopropyl-5-methylazepan-1-yl	90	6-isopropyl-2,4-dimethylazepan-1-yl
91	6-isopropyl-2,3-dimethylazepan-1-yl	92	3-isopropyl-4,6-dimethylazepan-1-yl	93	2-hydroxy-6-isopropylazepan-1-yl
94	2-hydroxy-6-isopropyl-3-methylazepan-1-yl	95	2-hydroxy-6-isopropyl-3,4-dimethylazepan-1-yl	96	2-hydroxy-6-isopropyl-4-methylazepan-1-yl
97	3-ethyl-4-methoxyphenyl	98	5-ethyl-2,3-dimethylcyclohexyl	99	indolizin-2-yl

100	8-ethylindolizin-2-yl	101	3-hydroxyindolizin-2-yl	102	8-ethyl-3-hydroxyindolizin-2-yl
103	3-hydroxy-8-isopropylindolizin-2-yl	104	8-isopropylindolizin-2-yl	105	6-ethylpyridin-2-yl
106	6-ethyl-5-hydroxypyridin-2-yl	107	6-ethyl-3-hydroxypyridin-2-yl	108	6-ethyl-3,5-dihydroxypyridin-2-yl
109	6-ethyl-4-methylpyridin-2-yl	110	6-isopropylpyridin-2-yl	111	6-isopropyl-4-methylpyridin-2-yl
112	3-hydroxy-6-isopropylpyridin-2-yl	113	5-hydroxy-6-isopropylpyridin-2-yl	114	3,5-dihydroxy-6-isopropylpyridin-2-yl
115	4-cyclobutyl-3-ethylphenyl	116	4-cyclobutyl-3-ethyl-5-methylphenyl	117	4-cyclobutyl-5-ethyl-2-hydroxyphenyl
118	4-cyclopropyl-3-ethylphenyl	119	4-cyclopropyl-3-ethyl-5-methylphenyl	120	4-cyclopropyl-5-ethyl-2-hydroxyphenyl
121	4-cyclopropyl-3-isopropylphenyl	122	4-cyclopropyl-3-isopropyl-5-methylphenyl	123	4-cyclopropyl-2-hydroxy-5-isopropylphenyl
124	4-cyclopropyl-2-hydroxy-5-isopropyl-3-methylphenyl	125	4-cyclopropyl-5-ethyl-2-hydroxy-3-methylphenyl	126	4-cyclobutyl-5-ethyl-2-hydroxy-3-methylphenyl
127	4-cyclopentyl-3-ethylphenyl	128	4-cyclopentyl-3-ethyl-5-methylphenyl	129	4-cyclopentyl-5-ethyl-2-hydroxy-3-methylphenyl
130	4-cyclopentyl-5-ethyl-2-hydroxyphenyl	131	4-cyclopentyl-3-isopropylphenyl	132	4-cyclopentyl-3-isopropyl-5-methylphenyl
133	4-cyclopentyl-2-hydroxy-5-isopropyl-3-methylphenyl	134	4-cyclopentyl-2-hydroxy-5-isopropylphenyl	135	4-(1H-pyrrol-1-yl)cyclohexyl
136	3-ethyl-4-(1H-pyrrol-1-yl)cyclohexyl	137	3-ethyl-5-methyl-4-(1H-pyrrol-1-yl)cyclohexyl	138	5-ethyl-2-hydroxy-4-(1H-pyrrol-1-yl)cyclohexyl
139	5-ethyl-2-hydroxy-3-methyl-4-(1H-pyrrol-1-yl)cyclohexyl	140	3-isopropyl-4-(1H-pyrrol-1-yl)cyclohexyl	141	3-isopropyl-5-methyl-4-(1H-pyrrol-1-yl)cyclohexyl
142	2-hydroxy-5-isopropyl-4-(1H-pyrrol-1-yl)cyclohexyl	143	2-hydroxy-5-isopropyl-3-methyl-4-(1H-pyrrol-1-yl)cyclohexyl	144	4-(furan-2-yl)cyclohexyl
145	3-ethyl-4-(furan-2-yl)cyclohexyl	146	3-ethyl-4-(furan-2-yl)-5-methylcyclohexyl	147	5-ethyl-4-(furan-2-yl)-2-hydroxycyclohexyl
148	5-ethyl-4-(furan-2-yl)-2-hydroxy-3-methylcyclohexyl	149	4-(furan-2-yl)-2-hydroxy-5-isopropyl-3-methylcyclohexyl	150	4-(furan-2-yl)-2-hydroxy-5-isopropylcyclohexyl
151	4-(furan-2-yl)-3-isopropyl-5-methylcyclohexyl	152	4-(azetidin-1-yl)-3-ethylphenyl	153	4-(azetidin-1-yl)-3-ethyl-5-methylphenyl
154	4-(azetidin-1-yl)-5-ethyl-2-hydroxyphenyl	155	4-(azetidin-1-yl)-5-ethyl-2-hydroxy-3-	156	4-(azetidin-1-yl)-3-isopropylphenyl

			methylphenyl		
157	4-(azetidin-1-yl)-3-isopropyl-5-methylphenyl	158	4-(azetidin-1-yl)-2-hydroxy-5-isopropylphenyl	159	4-(azetidin-1-yl)-2-hydroxy-5-isopropyl-3-methylphenyl
160	4-(aziridin-1-yl)-3-ethylphenyl	161	4-(aziridin-1-yl)-3-ethyl-5-methylphenyl	162	4-(aziridin-1-yl)-5-ethyl-2-hydroxy-3-methylphenyl
163	4-(aziridin-1-yl)-5-ethyl-2-hydroxyphenyl	164	4-(aziridin-1-yl)-3-isopropylphenyl	165	4-(aziridin-1-yl)-3-isopropyl-5-methylphenyl
166	4-(aziridin-1-yl)-2-hydroxy-5-isopropyl-3-methylphenyl	167	4-(aziridin-1-yl)-2-hydroxy-5-isopropylphenyl	168	3-methoxyphenyl
169	5-ethyl-2-methoxyphenyl	170	3-ethyl-5-methoxyphenyl	171	3-methoxycyclohexyl
172	5-ethyl-2-methoxycyclohexyl	173	3-ethyl-5-methoxycyclohexyl	174	5-ethyl-2-methoxypiperidin-1-yl
175	3-ethyl-5-methoxypiperidin-1-yl	176	3-methoxypiperidin-1-yl	177	6-ethyl-2-methoxycycloheptyl
178	3-ethyl-6-methoxycycloheptyl)	179	3-methoxycycloheptyl	180	6-ethyl-2-methoxyazepan-1-yl
181	3-ethyl-6-methoxyazepan-1-yl	182	3-methoxyazepan-1-yl	183	5-ethyl-2-methoxy-4-(1H-pyrrol-1-yl)phenyl
184	3-methoxy-4-(1H-pyrrol-1-yl)phenyl	185	5-ethyl-4-(furan-3-yl)-2-methoxyphenyl	186	4-(furan-3-yl)-3-methoxyphenyl
187	8-ethyl-3-methoxyindolizin-2-yl	188	8-ethyl-5-methoxyindolizin-2-yl	189	8-methoxyindolizin-2-yl
190	6-ethyl-3-methoxypyridin-2-yl	191	6-ethyl-4-methoxypyridin-2-yl	192	6-methoxypyridin-2-yl
193	4-cyclopropyl-5-ethyl-2-methoxyphenyl	194	4-cyclopropyl-3-ethyl-5-methoxyphenyl	195	4-cyclopropyl-3-methoxyphenyl
196	4-cyclobutyl-5-ethyl-2-methoxyphenyl	197	4-cyclobutyl-3-ethyl-5-methoxyphenyl	198	4-cyclobutyl-3-methoxyphenyl
199	4-cyclopentyl-5-ethyl-2-methoxyphenyl	200	4-cyclopentyl-3-methoxyphenyl	201	4-(azetidin-1-yl)-5-ethyl-2-methoxyphenyl
202	4-(azetidin-1-yl)-3-ethyl-5-methoxyphenyl	203	4-(azetidin-1-yl)-3-methoxyphenyl	204	4-(aziridin-1-yl)-5-ethyl-2-methoxyphenyl
205	4-(aziridin-1-yl)-3-ethyl-5-methoxyphenyl	206	4-(aziridin-1-yl)-3-methoxyphenyl	207	5-ethyl-2-methoxy-4-(pyrrolidin-1-yl)phenyl
208	3-methoxy-4-(pyrrolidin-1-yl)phenyl	209	5-ethyl-2-methoxy-4-(1H-pyrrol-1-yl)cyclohexyl	210	3-methoxy-4-(1H-pyrrol-1-yl)cyclohexyl

211	5-ethyl-4-(furan-2-yl)-2-methoxycyclohexyl	212	4-(furan-2-yl)-3-methoxycyclohexyl	213	5-ethyl-2-methoxy-4-(1H-pyrrol-1-yl)piperidin-1-yl
214	3-methoxy-4-(1H-pyrrol-1-yl)piperidin-1-yl	215	5-ethyl-4-(furan-2-yl)-2-methoxypiperidin-1-yl	216	4-(furan-2-yl)-3-methoxypiperidin-1-yl
217	3-ethyl-4-(1H-pyrrol-1-yl)piperidin-1-yl	218	5-ethyl-2-hydroxy-4-(1H-pyrrol-1-yl)piperidin-1-yl	219	3-ethyl-5-methyl-4-(1H-pyrrol-1-yl)piperidin-1-yl
220	3-ethyl-4-(furan-2-yl)piperidin-1-yl	221	3-ethyl-4-(furan-2-yl)-5-methylpiperidin-1-yl	222	5-ethyl-4-(furan-2-yl)-2-hydroxypiperidin-1-yl
223	6-ethylindolizin-8-yl	224	6-isopropylindolizin-8-yl	225	5-hydroxy-6-isopropylindolizin-8-yl
226	6-ethyl-5-hydroxyindolizin-8-yl	227	3-ethylnaphthalen-1-yl	228	3-ethylisoquinolin-1-yl
229	5-ethyl-1H-indol-1-yl	230	6-ethyl-1H-indol-1-yl	231	4-(1H-azirin-1-yl)-3-ethylphenyl
232	4-(1H-azirin-1-yl)-5-ethyl-2-hydroxyphenyl	233	4-(1H-azirin-1-yl)-5-ethyl-2-hydroxy-3-methylphenyl	234	5-(1H-azirin-1-yl)-6-ethyl-3-hydroxy-4-methylpyridin-2-yl
235	5-(1H-azirin-1-yl)-6-ethyl-3-hydroxypyridin-2-yl	236	5-(1H-azirin-1-yl)-6-ethyl-4-methylpyridin-2-yl	237	5-(1H-azirin-1-yl)-6-isopropyl-4-methylpyridin-2-yl
238	5-(1H-azirin-1-yl)-3-hydroxy-6-isopropyl-4- methylpyridin-2-yl	239	5-(1H-azirin-1-yl)-3-hydroxy-6-isopropylpyridin-2-yl	240	4-(1H-azirin-1-yl)-3-isopropylphenyl
241	4-(1H-azirin-1-yl)-2-hydroxy-5-isopropylphenyl	242	4-(1H-azirin-1-yl)-2-hydroxy-5-isopropyl-3-methylphenyl	243	3-methyldecahydronaphthalen-1-yl
244	3-ethyldecahydronaphthalen-1-yl	245	3-ethyloctahydroquinolin-1(2H)-yl	246	3-methyloctahydroquinolin-1(2H)-yl
247	3-methyloctahydroquinazolin-1(2H)-yl	248	3-ethyloctahydroquinazolin-1(2H)-yl	249	ethyl-formic acid-1-yl
250	methyl-formic acid-1-yl	251	methyl-formic amid-1-yl	252	ethyl-formic amid-1-yl
253	propyl-formic amid-1-yl	254	propyl-formic acid-1-yl	255	isobutyl-formic acid-1-yl
256	isobutyl-formic amid-1-yl	257	(1H-pyrrol-1-yl)methyl-formic acid-1-yl	258	(1H-pyrrol-1-yl)methyl-formic amid-1-yl
259	cyclobutylmethyl-formic acid-1-yl	260	azetidin-1-ylmethyl-formic acid-1-yl	261	cyclopropylmethyl-formic acid-1-yl
262	aziridin-1-ylmethyl-formic acid-1-yl	263	(1H-azirin-1-yl)methyl-formic acid-1-yl	264	cyclobutylmethyl-formic amid-1-yl

265	azetidin-1-ylmethyl-formic amid-1-yl	266	cyclopropylmethyl-formic amid-1-yl	267	aziridin-1-ylmethyl-formic amid-1-yl
268	(1H-azirin-1-yl)methyl-formic amid-1-yl	269	2-methylallyl-formic acid-1-yl	270	(2-methylallyl)-formic amid-1-yl
271	(4-methoxypiperidin-1-yl)methyl	272	(4-ethoxypiperidin-1-yl)methyl	273	((4-isopropoxypiperidin-1-yl))methyl)
274	(4-acetylpiperidin-1-yl)methyl	275	(4-propionylpiperidin-1-yl)methyl	276	(4-isobutyrylpiperidin-1-yl)methyl
277	(4-isobutylpiperidin-1-yl)methyl	278	(4-(pentan-3-yl)piperidin-1-yl)methyl	279	(4-methoxy-3-methylpiperidin-1-yl)methyl
280	(3-ethyl-4-methoxypiperidin-1-yl)methyl	281	(3-isopropyl-4-methoxypiperidin-1-yl)methyl	282	(3,4-dimethoxypiperidin-1-yl)methyl
283	(4-ethoxy-3-methylpiperidin-1-yl)methyl	284	(4-ethoxy-3-ethylpiperidin-1-yl)methyl	285	(4-ethoxy-3-isopropylpiperidin-1-yl)methyl
286	(4-ethoxy-3-methoxypiperidin-1-yl)methyl	287	(4-methoxyazepan-1-yl)methyl	288	(4-ethoxyazepan-1-yl)methyl
289	(4-isopropoxyazepan-1-yl)methyl	290	(3-isopropoxypyrrolidin-1-yl)methyl	291	(3-(methoxymethyl)pyrrolidin-1-yl)methyl
292	(3-(isopropoxymethyl)pyrrolidin-1-yl)methyl	293	(4-acetylazepan-1-yl)methyl	294	(4-propionylazepan-1-yl)methyl
295	(4-isobutyrylazepan-1-yl)methyl	296	(3-acetylpyrrolidin-1-yl)methyl	297	(3-propionylpyrrolidin-1-yl)methyl
298	(3-isobutyrylpyrrolidin-1-yl)methyl	299	(3-(3-oxopropyl)pyrrolidin-1-yl)methyl	300	(3-(2-methyl-3-oxopropyl)pyrrolidin-1-yl)methyl
301	(3-(3-oxobutyl)pyrrolidin-1-yl)methyl				

** R1-groups: 1 – 248; R2-groups: 249 – 270; R3-groups: 271 – 301.*

3.4.2 *In silico* screening of the virtual library

The screening of the downsized virtual library (10,919 analogs) has been carried out by the 3D-QSAR pharmacophore model of Pks13 inhibition. out of the screened analogs, 109 exhibiting at least four features of the pharmacophore have been picked. the free enthalpy complexation variation with respect to the reference ligand and its components has been computed and reported in the (Table 6). The predicted activity of 109 analogs has been computed with the QSAR equation of the aqueous-environment complexation.

Table 6. GFE and their components for the top scoring 109 virtual benzofuran analogs. The analog numbering concatenates the index of each substituent R1 to R3 with the substituent numbers taken from (Table 5)

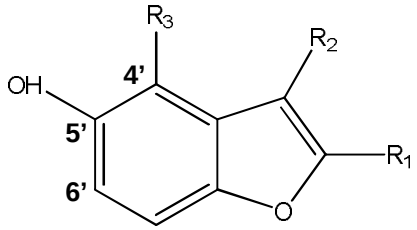

N°	Designed analogs	$\Delta\Delta H_{MM}$ [a] $[kcal.mol^{-}$	$\Delta\Delta G_{sol}$ [b] $[kcal.mol^{-1}]$	$\Delta\Delta TS_{vib}$ [c] $[kcal.mol^{-1}]$	$\Delta\Delta G_{com}$ [d] $[kcal.mol^{-1}]$	IC_{50}^{pre} [e] [nM]
Ref	TAM2	0.00	0.00	0.00	0.00	120.00
1	30-249-279	-8.06	1.74	1.92	-8.24	1.31
2	34-249-271	-14.73	7.60	-0.37	-6.76	2.76
3	108-249-283	-9 .07	2.04	0.81	-7.84	1.60
4	113-249-299	-10.14	2.13	0.26	-8.26	1.30
5	174-249-297	-7.74	3.90	3.29	-7.14	2.28
6	3-250-279	-14.65	7.54	-0.86	-6.25	3.56
7	13-250-279	-7.70	3.02	3.01	-7.68	1.73
8	18-250-288	-1.43	0.82	5.98	-6.58	3.01
9	21-250-280	-1.67	2.68	7.50	-6.49	3.15
10	33-250-279	-5.46	4.30	-1.97	0.82	123.87
11	62-250-287	-3.70	1.47	5.70	-7.93	1.53
12	93-250-287	-2.57	2.27	6.80	-7.10	2.32
13	106-250-283	-12.25	4.44	-0.10	-7.71	1.70
14	108-250-283	-8.33	1.86	-0.27	-6.20	3.65
15	27-250-296	-6.85	4.04	2.10	-4.91	6.97
16	113-250-279	-12.13	7.88	2.20	-6.45	3.22
17	171-250-297	-8.24	2.50	0.65	-6.39	3.31
18	172-250-279	-7.68	2.48	1.98	-7.18	2.23
19	172-250-290	-6.50	2.33	3.32	-7.50	1.90
20	30-250-290	-5.90	1.19	0.30	-5.02	6.61
21	190-250-281	0.95	2.79	1.86	1.88	211.34
22	192-250-299	-9.99	1.79	-2.42	-5.78	4.51
23	195-250-279	-15.64	8.58	0.00	-7.06	2.37
24	235-250-279	-3.07	2.90	-1.05	0.88	127.77
25	235-250-290	1.34	0.78	0.82	1.30	157.87
26	30-251-283	-7.98	1.84	-0.61	-5.53	5.09
27	5-251-297	-10.41	2.69	-0.72	-7.01	2.43
28	10-251-283	-9.45	2.16	-0.38	-6.91	2.55
29	11-251-279	-5.25	2.70	3.86	-6.40	3.30
30	18-251-279	-7.41	3.42	2.80	-6.79	2.71
31	21-250-285	5.00	2.13	5.87	1.26	155.07
32	23-251-279	-5.67	2.74	4.46	-7.39	2.01
33	24-250-298	-6.31	3.03	3.66	-6.94	2.51
34	27-251-283	-7.07	3.62	4.54	-7.98	1.49
35	31-251-293	-12.22	7.23	1.08	-6.08	3.87
36	31-251-298	-10.67	3.14	-0.81	-6.72	2.81
37	34-251-283	-14.20	8.15	0.70	-6.75	2.77

38	44-251-296	-9.04	6.81	-3.75	1.52	176.32

Nº	Designed analogs	$\Delta\Delta H_{MM}$ [a] $[kcal.mol^{-}]$	$\Delta\Delta G_{sol}$ [b] $[kcal.mol^{-1}]$	$\Delta\Delta TS_{vib}$ [c] $[kcal.mol^{-1}]$	$\Delta\Delta G_{com}$ [d] $[kcal.mol^{-1}]$	IC_{50}^{pre} [e] $[nM]$
39	60-251-290	-5.92	2.70	3.83	-7.04	2.39
40	82-251-274	-9.20	3.66	2.46	-8.00	1.47
41	82-251-283	-3.71	1.91	6.44	-8.24	1.31
42	87-251-297	-5.96	3.41	4.18	-6.73	2.79
43	93-251-279	-5.42	3.61	5.66	-7.47	1.93
44	105-251-283	-14.43	5.62	-1.11	-7.70	1.72
45	106-251-279	-14.85	6.76	-1.02	-7.07	2.36
46	108-251-283	-8.54	2.74	0.96	-6.76	2.75
47	110-251-283	-15.19	7.95	-0.32	-6.92	2.53
48	113-251-283	-12.68	7.17	0.68	-6.19	3.66
49	113-251-297	-9.43	2.72	0.98	-7.68	1.73
50	135-251-280	-1.01	4.88	1.20	2.67	313.68
51	163-251-279	-6.08	2.76	2.97	-6.30	3.47
52	171-251-279	-5.68	2.20	3.74	-7.22	2.18
53	172-251-297	-9.26	3.99	1.33	-6.60	2.98
54	191-251-279	-10.74	2.94	0.15	-7.96	1.51
55	206-251-283	-7.27	1.46	1.98	-7.79	1.64
56	223-251-298	-10.37	4.05	0.08	-6.40	3.30
57	224-251-297	-11.56	4.14	-0.22	-7.20	2.20
58	229-251-279	-15.62	9.23	0.32	-6.71	2.83
59	3-252-287	-7.02	2.25	3.36	-8.12	1.39
60	10-252-297	-12.16	3.03	-1.54	-7.58	1.82
61	53-252-286	-11.43	6.38	1.05	-6.10	3.84
62	55-252-296	-10.27	2.91	0.67	-8.03	1.45
63	82-252-297	-6.34	3.92	5.11	-7.53	1.87
64	110-252-300	-8.51	3.31	0.04	-5.25	5.89
65	100-252-279	-8.73	2.83	1.86	-7.77	1.66
66	105-252-298	-11.94	2.98	-1.78	-7.18	2.23
67	113-252-279	-13.71	8.49	1.27	-6.49	3.16
68	168-252-297	-8.13	2.78	-1.11	-4.24	9.77
69	189-252-279	-9.74	2.97	1.28	-8.05	1.44
70	192-252-298	-11.33	3.00	-0.43	-7.90	1.55
71	195-252-279	-15.47	9.50	1.74	-7.70	1.72
72	106-253-280	-15.13	9.06	1.37	-7.44	1.96
73	107-253-297	-9.88	3.57	1.27	-7.58	1.82
74	190-253-296	-10.12	3.23	-2.68	-4.22	9.88
75	206-253-271	-11.08	4.57	1.56	-8.07	1.43
76	99-254-299	-2.71	2.28	-0.45	0.02	83.12
77	176-254-279	-8.07	3.02	3.11	-8.16	1.36
78	192-254-297	-11.99	2.70	-1.43	-7.87	1.58
79	113-256-291	-7.45	4.58	4.25	-7.13	2.29
80	105-257-296	-15.63	7.45	-1.67	-6.51	3.12
81	120-258-291	-9.67	5.82	4.05	-7.90	1.55
82	192-259-279	-13.45	5.93	-1.17	-6.35	3.38
83	176-260-296	-9.80	3.37	1.00	-7.43	1.97
84	112-261-296	-8.56	2.82	-0.17	-5.57	5.01
85	113-261-291	-6.21	3.59	-2.02	-0.60	60.63
86	105-262-292	-5.79	2.64	-0.59	-2.57	22.62
87	4-263-279	-16.35	7.81	-2.51	-6.04	3.96
88	105-263-283	-0.33	1.30	-0.46	1.43	168.26

89	112-263-291	-1.62	2.61	-3.34	4.33	724.13

N°	Designed analogs	$\Delta\Delta\mathbf{H_{MM}}$ [a] $[\mathbf{kcal.mol^{-}}]$	$\Delta\Delta\mathbf{G_{sol}}$ [b] $[\mathbf{kcal.mol^{-1}}]$	$\Delta\Delta\mathbf{TS_{vib}}$ [c] $[\mathbf{kcal.mol^{-1}}]$	$\Delta\Delta\mathbf{G_{com}}$ [d] $[\mathbf{kcal.mol^{-1}}]$	$\mathbf{IC_{50}^{pre}}$ [e] $[\mathbf{nM}]$
90	107-264-291	-6.96	4.09	3.77	-6.63	2.93
91	110-265-291	-6.49	4.25	3.90	-6.13	3.77
92	1-266-298	-11.57	4.30	0.45	-7.71	1.71
93	56-267-279	-5.78	3.14	3.95	-6.59	2.99
94	179-267-297	-12.64	4.23	-0.31	-8.10	1.40
95	192-267-279	-17.92	8.41	-1.93	-7.58	1.82
96	2-268-296	-7.14	4.09	-6.10	3.05	381.13
97	11-268-280	1.23	3.56	4.05	0.74	119.27
98	20-268-271	-9.58	3.65	0.95	-6.87	2.60
99	53-268-296	-3.09	3.51	-1.83	2.25	254.43
100	105-268-283	-2.41	2.28	-0.54	0.41	100.94
101	113-268-296	-3.45	3.77	-1.70	2.02	226.39
102	168-269-279	-11.75	5.24	-0.15	-6.36	3.37
103	82-269-296	-5.05	3.57	4.80	-6.28	3.50
104	171-270-280	-4.52	2.79	5.09	-6.81	2.68
105	190-270-296	-12.14	3.71	-2.37	-6.06	3.92
106	24-250-279	-3.92	2.75	4.71	-5.88	4.28
107	209-250-296	-9.11	1.75	-1.51	-5.86	4.33
108	105-266-279	-14.26	8.63	0.23	-5.86	4.33
109	106-266-274	-21.11	11.14	-4.16	-5.81	4.44

[a] $\Delta\Delta H_{MM}$ *is the relative enthalpic contribution to the GFE change of the Pks13-TAM complex formation* $\Delta\Delta G_{com}$ *(for details see footnote of Table 2) ;* [b] $\Delta\Delta G_{sol}$ *is the relative solvation GFE contribution to ; c* $\Delta\Delta TS_{vib}$ *is the relative (vibrational) entropic contribution to* $\Delta\Delta G_{com}$ *; d* $\Delta\Delta G_{com}$ *is the relative Gibbs free energy (GFE) change related to the enzyme–inhibitor Pks13-TAM complex formation* $\Delta\Delta G_{com} = \Delta\Delta H_{MM} + \Delta\Delta G_{sol} - \Delta\Delta TS_{vib}$; [e] IC_{50}^{pre} *is the predicted inhibition potency towards Pks13; Experimental value* IC_{50}^{exp} *is given for the reference inhibitor TAM2 instead of the predicted value.*

3.4.3 *Analysis of novel benzofuran analogs substituents*

In this part of our study, the goal is to identify the substitutes which lead to new Pks13 benzofuran inhibitors of Mycobacterium tuberculosis and whose predicted biological activities are better than the ones proposed by Aggarwal *et al.* [11]. To this end, histograms have been plotted to indicate the occurrence rate of substitutes on locations R_1, R_2 et R_3 among the 109 leads given by the PH4 screening. These histograms revealed that the most frequent substitutes are (occurrence frequency between brackets): 113(8), 105(7), 192(5), 82(4), 106(4), 171(3), 176(4), 108(3), 172(3), 190 (3), 30 (3), 110 (3) in R_1 ; 3(33), 2(22), 4(13), 20(6), 1(5), 5(4), 6(3), 15(3), 18(3), 19(3), 22(3), in R_2; 9(29), 27(13), 13(14), 26(13), 28(6), 21(5), 10(5), 1(3), 17(3), 20(3), 29(3), in R_3.

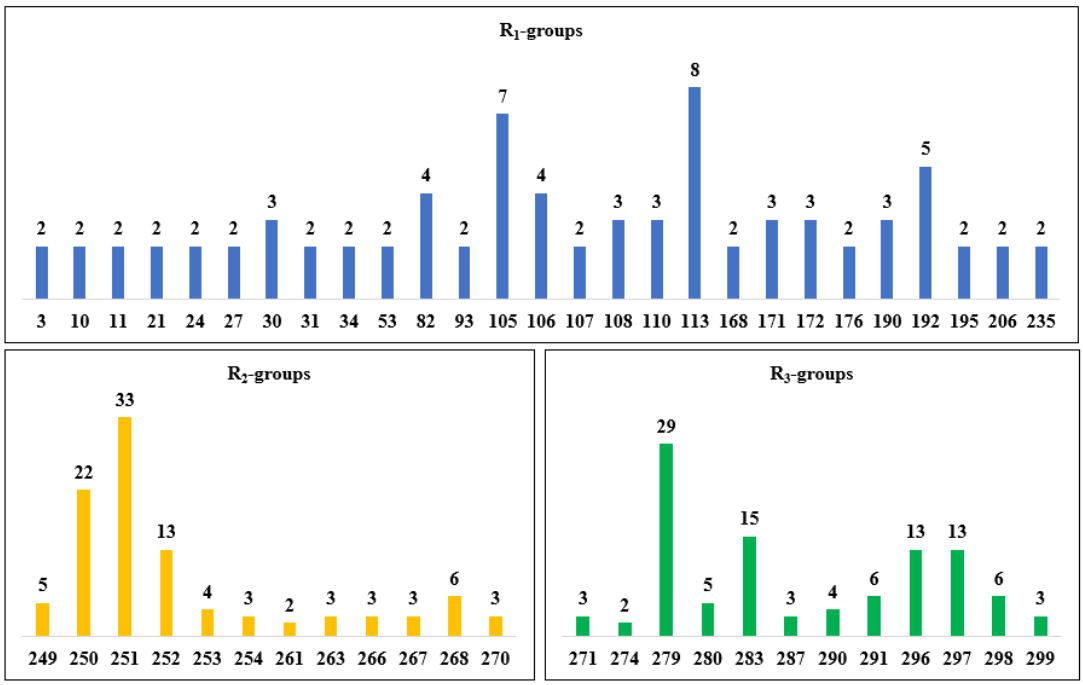

Fig. 5. Histograms of frequency of occurrence of individual R-groups in the 109 best-selected analogs mapping to features of the PH4 pharmacophore hypothesis Hypo1 (for the structures of the fragments see Table 5).

3.5 Pharmacokinetic Profile of New Benzofuran Analogs

The ADME (Absorption, Distribution, Metabolism, and Excretion) properties of a drug molecule such as: the octanol-water Partition Coefficient, the water-solubility, The brain-blood ratio (also referred to as the brain-plasma ratio), the permeability across Caco-2 cells, the binding to human serum albumin, the number of likely metabolic reactions and 18 other ADME-related descriptors of TAM analogues have been computed using the QikProp program [42]. This program is based on the Jorgensen method [38,43] and consists in using experimental data from more than 710 compounds, including about 500 drugs and heterocycles. The data has been used to fit regression models of the computed and experimental descriptors which in turn, enable us to precisely predict the pharmacokinetic properties of the designed molecules. The drug-likeness (number of stars) and the number of descriptive properties which fall outside the range of the optimal values determined for 95% of known drugs out of the 24 properties picked by QikProp have both been used as selection criteria in addendum to the ADME-related ones. The values of the descriptors of the pharmacokinetic properties of the best conceived benzofuran analogs are computed and then compared to those of the drugs which are currently used to treat tuberculosis or undergoing clinical trials (Table 7). The analysis of these computed descriptors (Table 7) indicates that the newly conceived benzofuran analogs are drug-like. Thus, these new TAM analogues are an excellent starting for the pharmaceutical industry in the discovery and development process towards new antituberculosis drugs. For most new analogs, the value associated to the drug-likeness descriptor (#star) is 0. Predictably, this indicates that no

criterion pertaining to the drug-likeness descriptors has been violated. Moreover, all these analogs have an acceptable oral absorption percentage (%HOA).

Table 7. Predicted ADME-related properties of 6 best designed benzofuran analogs and known antitubercular agents either in clinical use or currently undergoing clinical testing computed by QikProp [42]

TAMx [a]	#Stars [b]	Mw [c]	S_{mol} [d]	$S_{mol,hfo}$ [e]	V_{mol} [f]	RotB [g]	HBdon [h]	HBacc [i]	$logP_{o/w}$ [j]	$logS_{wat}$ [k]	$logK_{HSA}$ [l]	logB/B [m]	BIP_{caco} [n]	#meta [o]	IC_{50}^{Pre} [p]	HOA [q]	%HOA [r]
30-249-279	0	467.56	793.70	525.06	1467.46	8	2	7.70	4.37	-5.27	0.70	-0.25	563.42	6	1.31	3	100
3-252-287	0	480.60	825.57	598.96	1531.08	8	3	8.20	4.17	-5.56	0.72	-0.56	311.94	7	1.39	3	96
176-254-279	0	474.60	813.94	658.11	1511.83	8	1	9.15	4.19	-5.05	0.52	-0.01	932.77	4	1.36	3	100
179-267-297	0	497.63	863.00	672.06	1611.40	9	2	9.45	4.31	-5.68	0.69	-0.52	395.33	7	1.40	3	100
113-249-299	0	480.56	816.08	486.93	1514.85	10	2	9.00	3.41	-4.88	0.49	-1.44	67.34	8	1.30	3	100
82-251-283	0	487.64	844.22	662.99	1569.28	8	3	9.65	3.87	-5.41	0.56	-0.39	452.71	5	1.31	3	100
Rifampine	1	137	314	0.00	480 *	2	3	4.5	-0.7	0	-0.8	-0.80	267.5	2	-	2	67
Isoniazid	4	123.1 *	300	0.00	443 *	1	2	5	-0.6	-0.5	-0.8	-0.70	298.4	4	-	2	67
Ethambutol	2	204.3	476	395.80	806	11	4	6.4	-0.2	0.6	-0.8	0.00	107.8	4	-	2	62
Pyrazinamide	10	823.0 *	1090*	850.0 *	2300*	25 *	6	20.3 *	3.0	-3.1	-0.3	-2.70	38.2	11 *	-	1	34
Gatifloxacin	0	375.4	598	355.7	1093	2	1	6.8	0.5	-4.0	0	-0.60	17.00	1	-	2	52
Moxifloxacin	0	401.4	642	395.6	1168	2	1	6.8	1.0	-4.7	0.2	-0.60	20.90	1	-	2	56
Rifapentine	10	877.0*	1025*	844.9*	2333*	24*	6	20.9*	3.6	-2.2	-0.2	-1.50	224.40	13	-	1	51
Bedaquiline	4	555.5	787	213.7	1532	9	1	3.8	7.6*	-6.9	1.7	0.40	1562.2	5	-	1	100
Delamanid	2	534.5	796	284.4	1470	7	0	6.0	5.8	-7.6	1.0	-1.00	590.9	2	-	1	85
Linezolid	0	337.4	555	337.2	996	2	1	8.7	0.6	-2.0	-0.7	-0.50	507.0	2	-	3	79
Sutezolid	1	353.4	594	330.6	1047	2	1	7.5	1.3	-3.4	-0.4	-0.40	449.3	0	-	3	82
Ofloxacin	1	361.4	581	337.0	1044	1	0	7.3	-0.4	-2.8	-0.5	-0.40	25.9	1	-	2	50
Amikacin	14	585.6	739	350.3	1500	22*	17*	26.9*	-7.9*	-0.2	-2.1	-3.50	0.00	14*	-	1	0
Kanamycin	10	484.5	656	258.9	1291	17*	15*	227*	-6.7*	2.0	-1.4	-3.10	0.00	12*	-	1	0
Imipenem	0	299.3	487	259.1	880	8	3	7.2	1.0	-1.8	-0.7	-1.40	35.00	3	-	3	61
Amoxicillin	2	365.4	561	164.6	1033	6	4	8.0	-2.5	-0.8	-1.1	-1.50	1.00	5	-	1	12
Clavulanate	0	199.2	397	184.6	630	4	2	6.5	-0.8	0.3	-1.3	-1.30	13.3	2	-	2	42

[a] designed benzofuran analogs and known antituberculotic agents, Table 6 ; [b] drug likeness, number of property descriptors (24 out of the full list of 49 descriptors of QikProp, ver. 3.7, release 14) that fall outside of the range of values for 95% of known drugs; [c] molar mass in [g.mol $^{-1}$] (range for 95% of drugs: 130–725 g.mol $^{-1}$) [32] ; [d] total solvent-accessible molecular surface, in [Å^2] (probe radius 1.4 Å) (range for 95% of drugs: 300–1000 Å 2); [e] hydrophobic portion of the solvent-accessible molecular surface, in [Å^2] (probe radius 1.4 Å) (range for 95% of drugs: 0–750 Å 2); [f] total volume of molecule enclosed by solvent-accessible molecular surface, in [Å^3] (probe radius 1.4 Å) (range for 95% of drugs: 500–2000 Å^3); [g] number of non-trivial (not CX3), non-hindered (not alkene, amide, small ring) rotatable bonds (range for 95% of drugs: 0–15); [h] estimated number of hydrogen bonds that would be donated by the solute to water molecules in an aqueous solution. Values are averages taken over

several configurations, so they can assume non-integer values (range for 95% of drugs: 0.0–6.0); [i] *estimated the number of hydrogen bonds that would be accepted by the solute from water molecules in an aqueous solution. Values are averages taken over a number of configurations, so they can assume non-integer values (range for 95% of drugs : 2.0–20.0) ;* [j] *logarithm of partitioning coefficient between n-octanol and water phases (range for 95% of drugs : −2 to 6.5) ;* [k] *logarithm of predicted aqueous solubility, logS. S in [mol·dm^{-3}] is the concentration of the solute in a saturated solution that is in equilibrium with the crystalline solid (range for 95% of drugs: −6.0 to 0.5);* [l] *logarithm of predicted binding constant to human serum albumin (range for 95% of drugs: −1.5 to 1.5);* [m] *logarithm of predicted brain/blood partition coefficient (range for 95% of drugs: −3.0 to 1.2);* [n] *predicted apparent Caco-2 cell membrane permeability in Boehringer-Ingelheim scale in [nm s^{-1}] (range for 95% of drugs: < 25 poor, > 500 nm s^{-1} great);* [o] *number of likely metabolic reactions (range for 95% of drugs: 1–8);* [p] *predicted constants IC_{50}^{pre} , IC_{50}^{pre} was predicted from computed $\Delta\Delta G_{com}$ using the regression Equation (B) shown in (Table 3) ;* [q] *human oral absorption (1 = low, 2 = medium, 3 = high);* [r] *percentage of human oral absorption in gastrointestinal tract (<25% = poor, >80% = high); * star in any column indicates that the property descriptor value of the compound falls outside the range of values for 95% of known drugs.*

3.6 Binding Mode of New Inhibitors from *In Silico* Screening

Figure 6 shows respectively the mapping of the new analogues to the Pks13 inhibition pharmacophore, the binding mode and the Connolly surface of six of the best designed analogs. In the work of Wilson et al. [44] it was reported that the pocket where R_3 binds is the most buried pocket
and plays a significant role in molecular recognition. The piperidine group only partially occupies the cavity that extends into the TE catalytic site. Moreover, the works of Aggarwal et al. [17], and Wilson et al. [44] also indicated that the piperidine group was optimally located sandwiched between Tyr1663 and Tyr1674, and its protonated N appears to be a bifurcated hydrogen donor, forming an intra-molecular hydrogen bond with the R2 carbonyl oxygen and another with the side chain oxygen of Asn1640. Based on this information, the nitrogen position was maintained in all proposed substitutions for the R_3 location of the benzofuran scaffold. The approach adopted in our study made it possible to identify the fragments at the R_3 location which best probe the catalytic pocket containing the residues Ser1533, His1699. Among these fragments we can cite: (4-methoxy-3-methylpiperidin-1-yl)methyl (279); (4-ethoxy-3-methylpiperidin-1-yl)methyl (283) ; (3-(3-oxopropyl)pyrrolidin-1-yl)methyl (299); (4-methoxyazepan-1-yl)methyl (287) and (3-propionylpyrrolidin-1-yl)methyl (297). With these fragments, (4-methoxy-3-methylpiperidin-1-yl)methyl (279); (4-ethoxy-3-methylpiperidin-1-yl)methyl (283); (3-propionylpyrrolidin-1-yl)methyl (297); (3-(3-oxopropyl)pyrrolidin-1-yl)methyl (299), a hydrogen binding has been observed with the Ser1533 residues (figure 6). The fragments (4-methoxy-3-methylpiperidin-1-yl)methyl (279) ; (4-methoxyazepan-1-yl)methyl (287); (3-propionylpyrrolidin-1-yl)methyl (297) enter a hydrogen binding with residue His1699 and the fragments (4-ethoxy-3-methylpiperidin-1-yl)methyl (283); (3-(3-oxopropyl)pyrrolidin-1-yl)methyl (299) enter a π-alkyl and van der Waals interaction with the same residue.
The π-alkyl and π-Sigma interactions are created with these fragments and the Tyr1674 residue. The Tyr1663 residue yields the π-alkyl interactions, Van der Waals and carbon-hydrogen kind of hydrogen bindings with these fragments (Figure 6). Alkyl interactions are also observed between these fragments and residues Ala1647 and Ile1643. Also, van der Waals interactions are observed with residues such as Val1562. With the same approach which helped identifying R_3 fragments, the fragments which fit the pocket on location R_1 have been determined. Among these we can list: 4-hydroxy-3-isopropylphenyl (3); 6-ethyl-2-hydroxyazepan-1-yl (82); 5-ethyl-2-hydroxyphenyl (30), 3-methoxypiperidin-1-yl (176); 3-methoxycycloheptyl (179); 5-hydroxy-6-isopropylpyridin-2-yl (113). A hydrogen interaction has been observed between residue Asn1640 and the fragments 6-ethyl-2-hydroxyazepan-

1-yl (82); 5-ethyl-2-hydroxyphenyl (30) (Figure 6: 30-249-279; 82-251-283). This interaction has been signaled in the works of Wang et al [21]. The fragments, 6-ethyl-2-hydroxyazepan-1-yl (82); 5-ethyl-2-hydroxyphenyl (30); 4-hydroxy-3-isopropylphenyl (3) enter a π-alkyl interaction with residues Tyr1582, Trp1579. The Phe1670 residue enters π-alkyl and π- π stacking interactions with, respectively, fragment 3-methoxypiperidin-1-yl (176) and fragments 5-ethyl-2- hydroxyphenyl (30); 4-hydroxy-3-isopropylphenyl (3); 5-hydroxy-6-isopropylpyridin-2-yl (113). The Ser1636 residue enters amide- π stacking interactions with fragments 5-ethyl-2-hydroxyphenyl (30). The fragments located on R_2 have been determined through the same approach as those of R_1 et R_2. We can cite the following as identified fragments on location R_2: ethyl-formic acid-1-yl (249); methyl-formic amid-1-yl (251); ethyl-formic amid-1-yl (252); propyl-formic acid-1-yl (254); aziridin-1-ylmethyl-formic amid-1-yl (267). When it comes to the six among the best analogs which are presented in (figure 6), the methyl-formic amid-1-yl (251) fragment; ethyl-formic amid-1-yl (252);propyl-formic acid-1-yl (254); aziridin-1-ylmethyl-formic amid-1-yl (267) and the Asn1640 residue contract a hydrogen binding. A π-alky interaction is often observed between the His1664 residue and the ethyl-formic acid-1-yl (249); propyl-formic acid-1-yl (254) fragments. Interactions with the benzofuran scaffold and residues Phe1670, Tyr1582, Asn1640 have been preserved.

All these observed interactions, whose hydrogen bindings with catalytic residues Ser1533 and His1699 along with residue Asn1640 as described in the works of Wang et al., justify the activity of the new analogs : 30-249-279 (IC_{50}^{pre} = 1.31nM) ; 3-252-287 (IC_{50}^{pre} = 1.39nM) ; 176-254-279 (IC_{50}^{pre} = 1.36nM) ; 179-267-297 (IC_{50}^{pre} = 1.40nM) ; 82-251-283 (IC_{50}^{pre} = 1.31nM) ; 113-249-299 (IC_{50}^{pre} = 1.30nM).

30-249-279(IC_{50}^{pre} = 1.31nM)

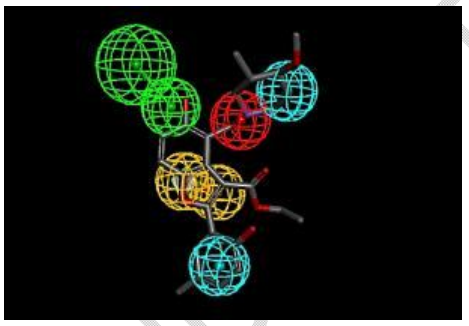

82-251-283 (IC_{50}^{pre} = 1.31nM)

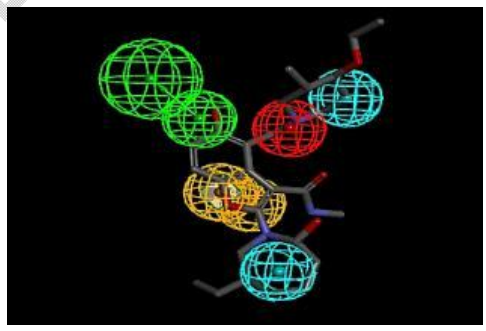

113-249-299 (IC_{50}^{pre} = 1.30nM)

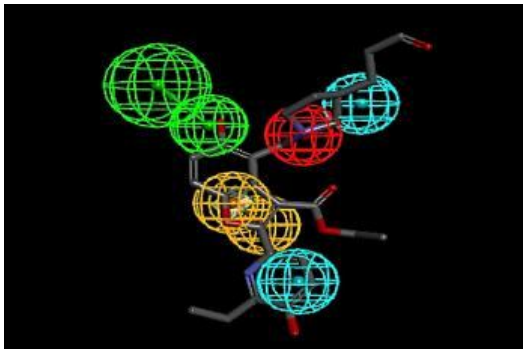

179-267-297 (IC_{50}^{pre} = 1.40nM)

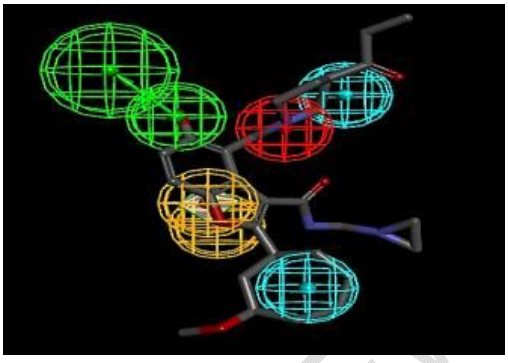

3-252-287 (IC_{50}^{pre} = 1.39nM)

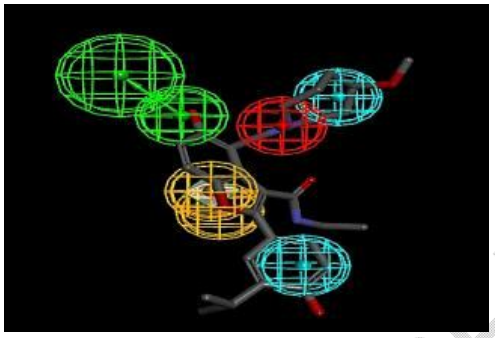

176-254-279 (IC_{50}^{pre} = 1.36nM)

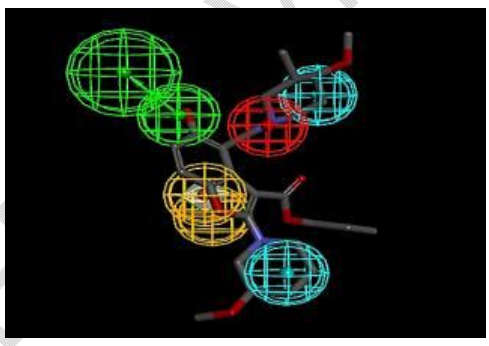

30-249-279(IC_{50}^{pre} = 1.31nM)

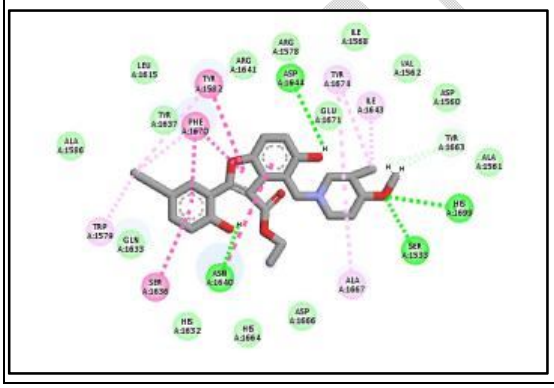

82-251-283 (IC_{50}^{pre} = 1.31nM)

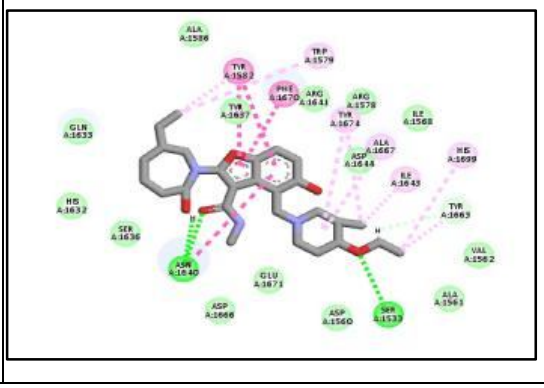

113-249-299 (IC_{50}^{pre} = 1.30nM)

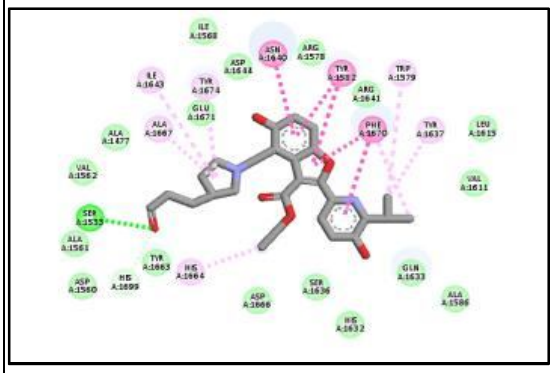

179-267-297 (IC_{50}^{pre} = 1.40nM)

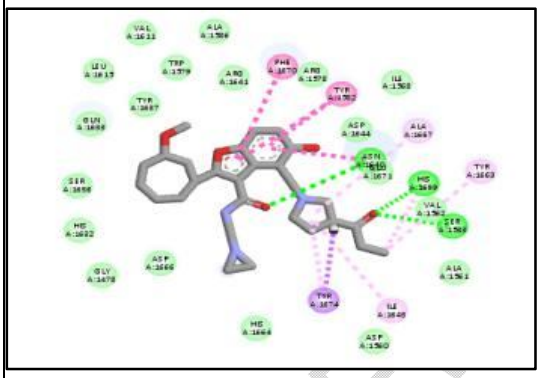

3-252-287 (IC_{50}^{pre} = 1.39nM)

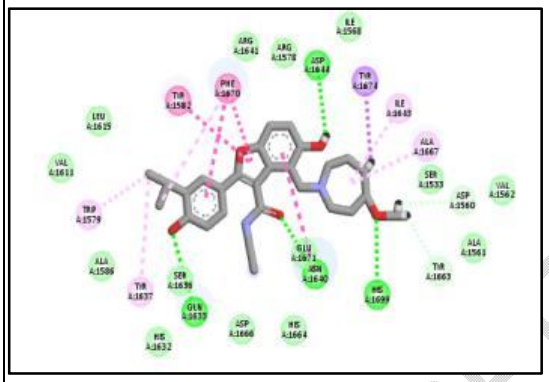

176-254-279 (IC_{50}^{pre} = 1.36nM)

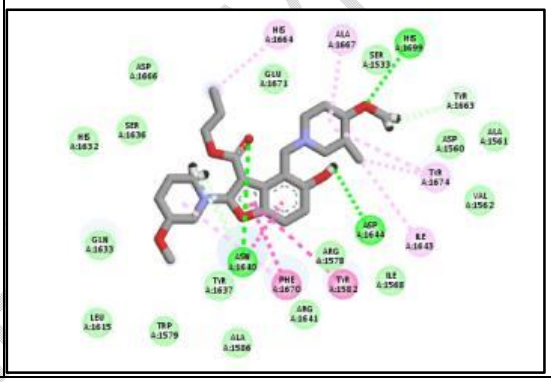

Van der

Conventional Hydrogen Bond

Carbon Hydrogen Bond

Pi-Pi Tshaped

Pi-Pi Stacked

Amide-Pi Stacked

Pi-Alkyl

Alkyl

Pi-Sigma

30-249-279(IC_{50}^{pre} = 1.31nM)

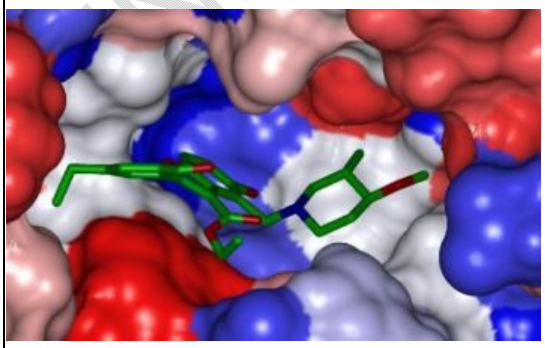

82-251-283 (IC_{50}^{pre} = 1.31nM)

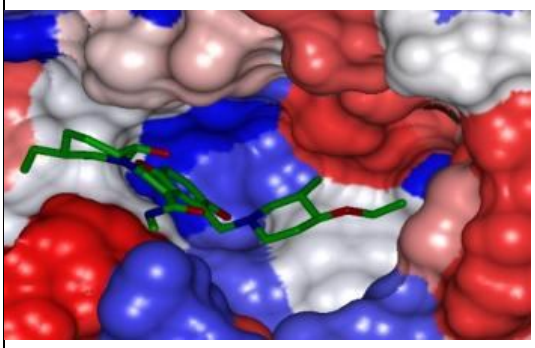

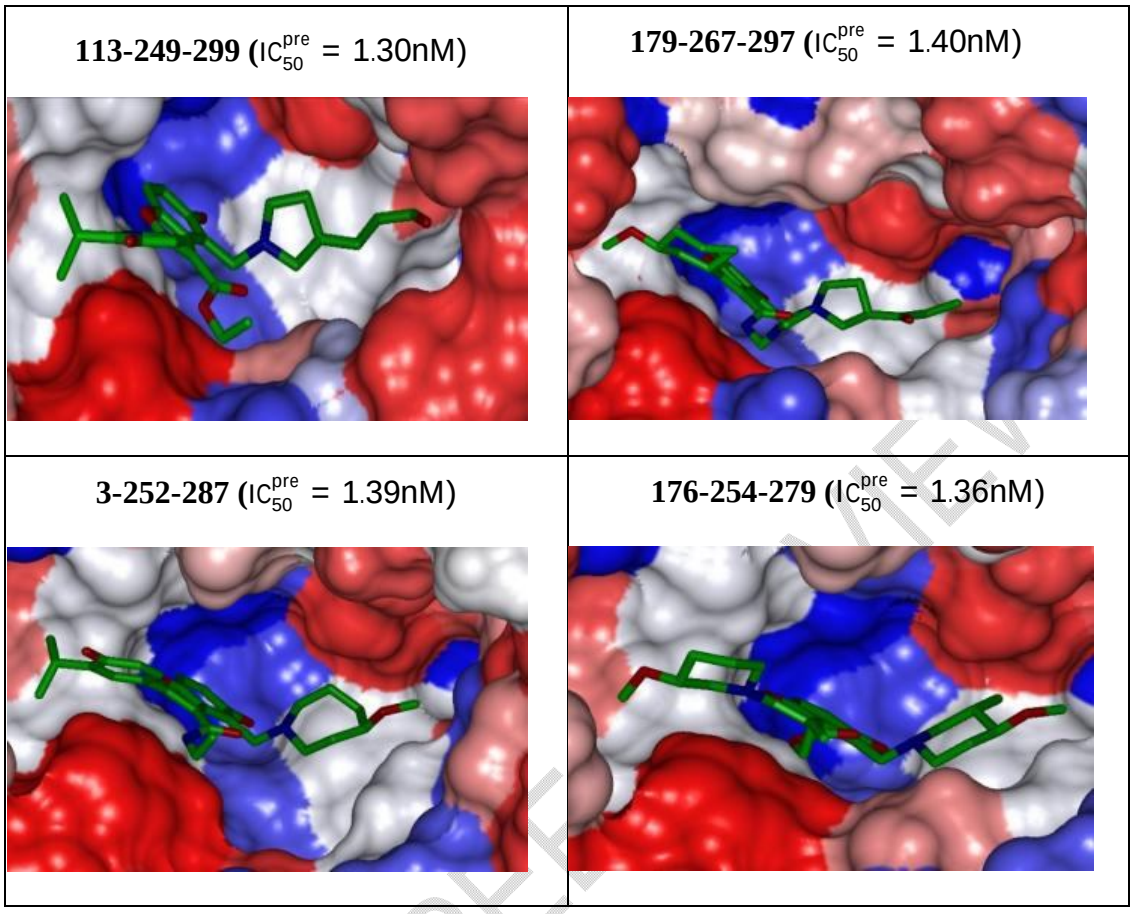

Fig. 6. Mapping of analogs 30-249-279; 3-252-287; 176-254-279; 82-251-283; 179-267-297; 113-249-299 to Pks13 inhibition pharmacophore, 2D schematic interaction diagram of the analogs 30-249-279; 3-252-287; 176-254-279; 82-251-283; 179-267-297; 113-249-299, Connolly surface of the active site of Pks13 with bound benzofuran analogs 30-249-279; 3-252-287; 176-254-279; 82-251-283; 179-267-297; 113-249-299. The binding site surface is coloured according to residue hydrophobicity: red - hydrophobic, blue – hydrophilic and white – intermediate.

3.7 Interaction Energy of New Inhibitors from *In Silico* Screening

The visual analysis of the new designed Pks13-TAMs complexes reveals that several residues of the Pks13 active site including catalytic residues, interact with the new analogues. These residues play a key role in the significant improvement of the inhibitive activity of the new analogues of benzofuran derivatives. The individual contributions of these residues in terms of interaction energy are represented by the diagram below (Figure 7). From the diagram, we can notice that residues Asn1640, Phe1670, Asp1644, Tyr1637, Tyr1582, Tyr1674, Gln1633, Ser1636, Glu1671, Tyr1663, Asp1666, Ala1667, His1632, Ile1643, Val1562, Trp1579 and catalytic residues His1699 and Ser1533. Unlike the ligands of the training set, the new analogs have a lower interaction energy with catalytic residues Ser1533 et His1699. This demonstrates a strong affinity of these residues for the fragments (279) : (4-methoxy-3-methylpiperidin-1-yl)methyl; (283): (4-ethoxy-3-methylpiperidin-1-

yl)methyl; (287): (4-methoxyazepan-1-yl)methyl; (297): (3-propionylpyrrolidin-1-yl)methyl; (299): (3-(3-oxopropyl)pyrrolidin-1-yl)methyl of the analogs designed: 30-249-279 (IC_{50}^{pre} = 1.31nM); 3-252-287 (IC_{50}^{pre} = 1.39nM); 176-254-279 (IC_{50}^{pre} = 1.36nM); 179-267-297 (IC_{50}^{pre} = 1.40nM); 82-251-283 (IC_{50}^{pre} = 1.31nM); 113-249-299 (IC_{50}^{pre} = 1.30nM). With the same fragments, the interaction energy between the best analogs and the residues Tyr1674 et Tyr1663 is lower than that scored by the training set ligands. The interaction energy between the new analogs and the Val1562 and Trp1579 residues is significant, more than the training set ligands. The contribution in terms of interaction energy of residues Tyr1582 and Gln1633 has decreased for fragments (113): 5-hydroxy-6-isopropylpyridin-2-yl; (82): 6-ethyl-2-hydroxyazepan-1-yl; (30): 5-ethyl-2-hydroxyphenyl; (3): 4-hydroxy-3-isopropylphenyl; (176): 3-methoxypiperidin-1-yl; (179): 3-methoxycycloheptyl of the R1 position. Also, the interaction energy of the Tyr1637 residues for fragments (82): 6-ethyl-2-hydroxyazepan-1-yl; (30): 5-ethyl-2-hydroxyphenyl; (176): 3-methoxypiperidin-1-yl; (179): 3-methoxycycloheptyl of the R_1 position decreased contrarily to that of the training set ligands. Generally, all fragments employed in the conception of better analogs enabled to improve interactions between the new analogs and the residues of the Pks13 active site, especially key residues like Asn1640, Phe1670, Asp1644, Ser1636 from Pks13 active site. All these observations about the individual contribution of interaction energy of the active site residues and of the catalytic residues, confirm the improved potency of the best designed analogs relative to TAM2.

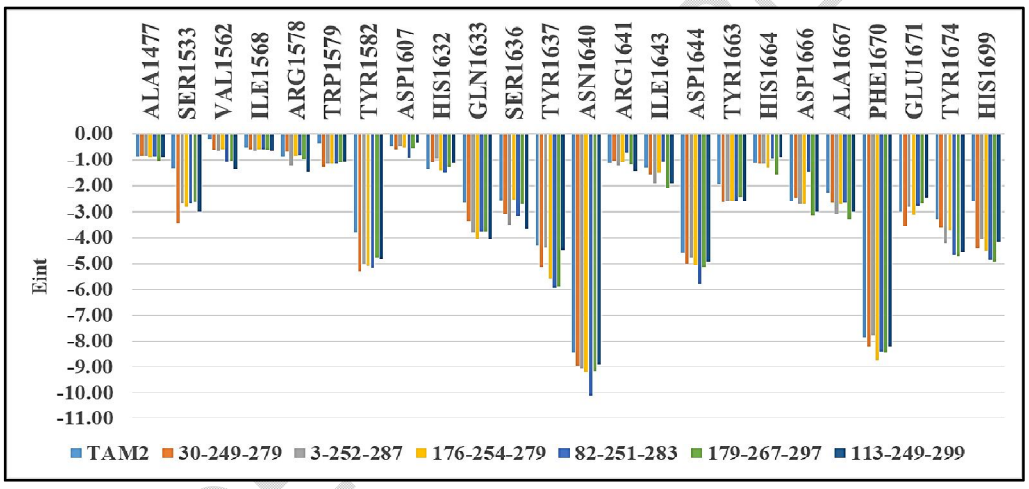

Fig. 7. Molecular mechanics intermolecular interaction energy E_{int} breakdown to residue contributions, in [kcal.mol^{-1}] shown for the best six designed novels benzofuran analogs (the color coding refers to ligands and is given in the legend).

4. CONCLUSION

Pks13 is a promising target in the development of and the search for new antituberculosis drugs due to its role in the final step of the mycolic acids' synthesis [17].

The structural properties of benzofuran derivatives identified by Aggarwal et al. [17] as potential antitubercular agent, and whose target is Pks13, enabled us to elaborate a QSAR complexation model able to explain more than 98% of the variation of the experimental inhibitory activity of the benzofuran derivatives by the Gibbs free energy of the Pks13-TAMs complex formation. Moreover, the subsequent pharmacophore model of Pks13 inhibition explains more than 90% of the variation of the experimental inhibitory activity by the

estimated activity at the generation step. The analysis of the interaction mode of the benzofuran derivatives at the Pks13 active site suggested substitutions at locations R_1, R_2 and R_3 in the enumeration of a combinatorial virtual library which has been focused according to Lipinski's rule of five and then screened by the pharmacophore to a handful of novel analogs the best of which are listed as follows: 30-249-279 (IC_{50}^{pre} = 1.31nM) ; 3-252-287 (IC_{50}^{pre} = 1.39nM) ; 176-254-279 (IC_{50}^{pre} = 1.36nM) ; 179-267-297 (IC_{50}^{pre} = 1.40nM) ; 82-251-283 (IC_{50}^{pre} = 1.31nM) ; 113-249-299 (IC_{50}^{pre} = 1.30nM).
On top of their activities, these molecules exhibit favorable predicted pharmacokinetic profile and are worth undergoing synthesis and biological evaluation.

ABBREVIATIONS

ADME	Absorption, Distribution, Metabolism, and excretion
2D	Two-dimensional
3D	Three-dimensional
Ar	Aromatic ring
E_{int}	MM enzyme–inhibitor interaction energy per residue
$\Delta\Delta G_{com}$	Relative complexation GFE
GFE	Gibbs free energy
$\Delta\Delta G_{sol}$	Relative solvation GFE
$\Delta\Delta TS_{vib}$	Relative entropic GFE
HBA	Hydrogen bond Acceptor
HBD	Hydrogen bond Donor
$\Delta\Delta H_{MM}$	Enthalpy component of GFE
IC_{50}	Half-maximal inhibitory concentration
LOO	Leave-one-out cross-validation
MM	Molecular mechanics
PDB	Protein Data Bank
PH4	Pharmacophore
Pks	Polyketide synthase
QSAR	Quantitative Structure-Activity Relationships
RMSD	Root-Mean Square Deviation
TE	Thioesterase
TS	Training set
VLC	Virtual combinatorial library
VS	Validation set

REFERENCES

1. Chiaradia L, Lefebvre C, Parra J, Marcoux J, BurletSchiltz O, Etienne G, et al. Dissecting the mycobacterial cell envelope and defining the composition of the native mycomembrane. Scientific Reports. 2017; 7:1-12. Available: doi:10.1038/s41598-017-12718-4.
2. Churchyard G, Kim P, Shah NS, Rustomjee R, Gandhi N, Mathema B, et al. What We Know About Tuberculosis Transmission: An Overview. The Journal of Infectious Diseases. 2017; 216: 629-35.
3. Dutta NK, Karakousis PC. Latent tuberculosis infection: myths, models, and molecular mechanisms. Microbiology and Molecular Biology Reviews. 2014; 78(3): 343-71. Available: doi:10.1128/MMBR.00010-14.
4. Golden MP, Vikram HR. Extrapulmonary Tuberculosis: An Overview. American Family Physician 2005; 72 (9): 1761-8.

5. World Health Organization. Global tuberculosis report 2021. (accessed 2022/05/25). Available: https://www.wipo.int/amc/fr/mediation/rules/index.html.
6. World Health Organization. Global tuberculosis report 2020. (accessed 2021/12/13). Available: https://apps.who.int/iris/handle/10665/336069.
7. Goldman RC. Why are membrane targets discovered by phenotypic screens and genome sequencing in Mycobacterium tuberculosis? Journal tuberculosis. 2013;93(6): 569-588. Available: https://doi.org/10.1016/j.tube.2013.09.003.
8. Druszczynska M, Kowalski K, Wawrocki S, Fol M. Diversity and functionality of Mycobacterial mycolic acids in relation to host-pathogen interactions. Current Medicinal Chemistry. 2017;24(38):4267-4278. Available: https://doi.org/10.2174/0929867324666170823130445.
9. Marrakchi H, Lanéelle MA, Daffé M. Mycolic acids: structures, biosynthesis, and beyond. Chemistry&Biology. 2014; 21(1):67-85. Available: https://doi.org/10.1016/j.chembiol.2013. 11.011.
10. Portevin D, De Sousa-D'Auria C, Houssin C, Grimaldi M, Chami M, Daffé M, et al. A polyketide synthase catalyzes the last condensation step of mycolic acid biosynthesis in mycobacteria and related organisms. The Proceeding of the National Academy of sciences. U.S.A. 2004; 101(1): 314-319. Available: https://doi.org/10.1073/pnas.0305439101.
11. Gavalda S, Bardou F, Laval F, Bon C, Malaga W, Chalut C, et al. The polyketide synthase Pks13 catalyzes a novel mechanism of lipid transfer in mycobacteria. Chemistry & Biology. 2014;21(12): 1660-1669. Available: https://doi.org/10.1016/j.chembiol.2014.10.011.
12. Wilson R, Kumar P, Parashar V, Vilchèze C, Veyron-Churlet R, Freundlich JS, et al. Antituberculosis thiophenes define a requirement for Pks13 in mycolic acid biosynthesis. Nature Chemical Biology. 2013; 9 499–506. Available: https://doi.org/10.1038/nchembio.1277.
13. Thanna S, Knudson SE, Grzegorzewicz A, Kapil S, Goins CM, Ronning DR, et al. Synthesis and evaluation of new 2-ami-nothiophenes against Mycobacterium tuberculosis. Organic Biomolecular Chemistry. 2016; 14(25): 6119–6133. Available: https://doi.org/10.10 39/C6OB00821F.
14. Lehmann J, Cheng TY, Aggarwal A, Park AS, Zeiler E, Raju RM, et al. An antibacterialB-lactone kills Mycobacterium tuberculosis by disrupting mycolic acid biosynthesis. Angewandte Chemie International Edition. 2018; 57(1): 348-353. Available: https://doi.org/10.1002/anie.201709365.
15. Goins CM, Sudasinghe TD, Liu X, Wang Y, O'Doherty GA, Ronning DR, et al. Characterization of tetrahydrolipstatin and stereoderivatives on the inhibition of essential Mycobacterium tuberculosis lipid esterases. Biochemistry. 2018; 57(16):2383–2393. Available: https://doi.org/10.1021/acs.biochem.8b00152.
16. Ioerger TR, O'Malley T, Liao R, Guinn KM, Hickey MJ, Mohaideen N, et al. Identification of new drug targets and resistance mechanisms in Mycobacterium tuberculosis. PLoS One. 2013 ; 8(9) :1-13. Available : https://doi.org/10.1371/journal.pone.0075245.
17. Aggarwal A, Parai MK, Shetty N, Wallis D, Woolhiser L, Hastings C, et al. Development of a novel lead that targets M. tuberculosis polyketide synthase 13. 2017; 170(2): 249-259. Available: https://doi.org/10.1016/j.cell.2017.06.025.
18. Zhang W, Lun S, Wang SH, Jiang XW, Yang F, Tang J, et al. Identification of novel coumestan derivatives as polyketide synthase 13 inhibitors against Mycobacterium tuberculosis, Journal of Medicinal Chemistry. 2018; 61(3): 791–803. Available: https://doi.org/10.1021/acs.jmedchem.7b01319.
19. Zhang W, Lun S, Liu LL, Xiao S, Duan G, Gunosewoyo H, et al. Identification of novel coumestan derivatives as polyketide synthase 13 inhibitors against Mycobacterium tuberculosis. Part II. Journal of Medicinal Chemistry. 2019; 62(7): 3575–3589. Available: https://doi.org/10.1021/acs.jmedchem.9b00010.

20. Zhao W, Wang B, Liu Y, Fu L, Sheng L, Zhao H, et al. Design, synthesis, and biological evaluation of novel 4H-chromen-4-one derivatives as antituberculosis agents against multidrug-resistant tuberculosis. European Journal of Medicinal chemistry. 2020; 189:1-14. Available: https://doi.org/10.1016/j.ejmech.2020.112075.
21. Wang X, Zhao W, Wang B, Ding W, Guo H, Zhao H, et al. Identification of inhibitors targeting polyketide synthase 13 of Mycobacterium tuberculosis as antituberculosis drug leads. Bioorganic Chemistry. 2021;114: 1-10. Available: https://doi.org/10.1016/j.bioorg. 2021.105110.
22. Accelrys Inc. Insight-II and Discover Molecular Modeling and Simulation Package, Release 2005; Accelrys Inc.: San Diego, CA, USA, 2005.
23. N'Guessan H, Megnassan E. In silico Design of Phosphonic Arginine and Hydroxamic Acid Inhibitors of Plasmodium falciparum M17 Leucyl Aminopeptidase with Favorable Profile. Journal of Drug Design and Medicinal Chemistry. 2017; 3:86-113. Available: doi: 10.11648/j.jddmc.20170306.13. View Article
24. Dali B, Keita M, Megnassan E, Frecer V, Miertus S. Insight into Selectivity of Peptidomimetic Inhibitors with Modified Statine Core for Plasmepsin II of Plasmodium falciparum over Human Cathepsin D. Chemical Biology & Drug Design. 2012; 79:411-430. PMid:22129033. View Article PubMed/NCBI.
25. Eknamkul W, Umehara K, Monthakantirat O, Toth R, Frecer V, Knapic L, et al. QSAR study of natural estrogen-like isoflavonoids and diphenolics from Thai medicinal plants. Journal of Molecular Graphics and Modelling. 2011;29:784-794. PMid:21334935. View Article PubMed/NCBI.
26. Esmel A, Keita M, Megnassan E, Toï B, Frecer V, Miertus S. Insight into binding mode of nitrile inhibitors of Plasmodium falciparum Falcipain-3, QSAR and Pharmacophore models, virtual design of new analogues with favorable pharmacokinetic profiles. Journal of Computational Chemistry & Molecular Modeling. 2017; 2:103-124. View Article
27. Frecer V, Berti F, Benedetti F, Miertus S. Design of peptidomimetic inhibitors of aspartic protease of HIV-1 containing -PheΨPro- core and displaying favorable ADME-related properties. Journal of Molecular Graphics and Modelling. 2008; 27:376-387.PMid:18678515. View Article PubMed/NCBI.
28. Frecer V, Burello E, Miertus S. Combinatorial design of nonsymmetrical cyclic urea inhibitors of aspartic protease of HIV-1. Bioorganic & Medicinal Chemistry. 2005; 13:5492-5501. PMid:16054372. View Article PubMed/NCBI
29. Frecer V, Megnassan E, Miertus S. Design and in silico screening of combinatorial library of antimalarial analogs of triclosan inhibiting Plasmodium falciparum enoyl-acyl carrier protein reductase. European Journal of Medicinal Chemistry. 2009; 44:3009-3019.PMid:19217192. View Article PubMed/NCBI
30. Frecer V, Miertus S,Tossi A, Romeo D. Rational design of inhibitors for drug resistant HIV-1 aspartic protease mutants. Drug design and discovery. 1998; 15:211-231.
31. Megnassan E, Keita M, Bieri C, Esmel A, Frecer V, Miertus S. Design of Novel Dihydroxynaphthoic Acid Inhibitors of Plasmodium Falciparum Lactate Dehydrogenase. Medicinal Chemistry. 2012; 8:970-984. PMid:22741776 View Article PubMed/NCBI
32. Owono LC, Keita M, Megnassan E, Frecer V, Miertus S. Design of Thymidine Analogues Targeting Thymidilate Kinase of Mycobacterium tuberculosis. Tuberculosis Research and Treatment. 2013; 2013: 670836. Available: doi:10.1155/2013/670836. PMid:23634301 View Article PubMed/NCBI

33. Owono Owono LC, Ntie-Kang F, Keita M, Megnassan E, Frecer V, Miertus S. Virtually Designed Triclosan-Based Inhibitors of Enoyl-Acyl Carrier Protein Reductase of Mycobacterium tuberculosis and of Plasmodium falciparum. Molecular Informatics. 2015; 34:292-307. Available: doi:10.1002/ minf.201400141. PMid:27490275 View Article PubMed/NCBI
34. Gilson MK, Honig B. The inclusion of electrostatic hydration energies in molecular mechanics calculations. Journal of Computer-Aided Molecular Design. 1991; 5:5-20. Available: doi:10.1007/BF00173467. PMid:2072125 View Article PubMed/NCBI
35. Rocchia W, Sridharan S, Nicholls A, Alexov E, Chiabrera A, Honig B. Rapid grid-based construction of the molecular surface and the use of induced surface charge to calculate reaction field energies: Applications to the molecular systems and geometric objects. Journal of Computational Chemistry. 2002; 23:128-137. PMid:11913378 View Article PubMed/NCBI
36. Allangba KNGPG, Keita M, Kre NR, Megnassan E, Frecer V, Miertus S. Virtual design of novel Plasmodium falciparum cysteine protease falcipain-2 hybrid lactone-chalcone and isatin-chalcone inhibitors probing the S2 active site pocket. J Enzyme Inhib Med Chem. 2019; 34: 547-561. Available: doi:1080/14756366.2018.1564288. PMid:30696325 View Article PubMed/NCBI
37. Li H, Sutter J, Hoffmann R. HypoGen: an automated system for generating 3D predictive pharmacophore models. Pharmacophore perception, development, and use in drug design. 2000; 2:171.
38. Jorgensen W, Duffy E. Prediction of drug solubility from Monte Carlo simulations. Bioorganic & Medicinal Chemistry Letters. 2000; 10(11):1155-1158. 00172-4 View Article
39. Discovery Studio molecular modeling and simulation program, version 2.5, Accelrys, Inc., San Diego, CA, California. USA. 2009.
40. Kouassi AF, Kone M, Keita M, Esmel A, Megnassan E, N'Guessan Y, et al. Computer-aided design of orally bioavailable pyrrolidine carboxamide inhibitors of Enoyl-Acyl Carrier Protein Reductase of Mycobacterium tuberculosis with favorable pharmacokinetic profiles. International Journal of Molecular Sciences. 2015; 16:29744-29771. PMid: 26703572 View Article PubMed/NCBI
41. Lipinski C, Lombardo F, Dominy B, Feeney P. Experimental and computational approaches to estimate solubility and permeability in drug discovery and development settings, Adv. Drug Deliv. Rev., 2001; 46: 3–26.
42. QikProp, version 3.7, release 14, X Schrödinger, LLC. New York, NY. 2014.
43. Jorgensen W and Duffy E. Prediction of drug solubility from structure. Advanced Drug Delivery Reviews. 2002; 54 (3):355–366. 00008-X View Article.
44. Wilson C, Ray P, Zuccotto F, Hernandez J, Aggarwal A, Mackenzie C, et al. Optimization of TAM16, a Benzofuran That Inhibits the Thioesterase Activity of Pks13; Evaluation toward a Preclinical Candidate for a Novel Antituberculosis Clinical Target. J. Med.Chem. 2022; 65:409−423. Available: https://doi.org/10.1021/acs.jmedchem.1c01586.